Diatom–environment relationships and limnological variability: an updated quantitative tool for palaeoclimatological studies on sub-Antarctic Macquarie Island

Caitlin A. Selfe[1], Karina Meredith[2], Liza McDonough[2], Justine Shaw[1], Stephen J. Roberts[3], Krystyna M. Saunders[2,4,5]

[1] Securing Antarctica's Environmental Future, Queensland University of Technology, Brisbane, 4000, Australia
[2] Securing Antarctica's Environmental Future, Environment Research and Technology Group, Australian Nuclear Science and Technology Organisation, Lucas Heights, 2234, Australia
[3] British Antarctic Survey, Cambridge, CB3 0ET, United Kingdom
[4] Institute for Marine and Antarctic Studies, University of Tasmania, Hobart, 7004, Australia
[5] Australian Antarctic Division, Kingston, 7050, Australia

Correspondence to: Caitlin A. Selfe (caitlin.selfe@hrd.qut.edu.au)

Keywords: Diatoms, Electrical conductivity, sub-Antarctic, Macquarie Island, Transfer function, Southern Hemisphere westerly winds, Palaeoclimate, Limnology

Commented [KS1]: I'm not sure whether you can still change the title, but should the word "studies" or "palaeoclimatological studies" be included?

Abstract. Sub-Antarctic Macquarie Island is ideally located for reconstructing past variations in Southern Hemisphere westerly wind strength. Diatoms are a valuable palaeolimnological tool on sub-Antarctic islands, providing a means to reconstruct past climate and environmental changes. Diatom communities are sensitive to changes in lake electrical conductivity (EC) linked to westerly wind–driven sea-spray inputs on Macquarie Island, and diatom–conductivity models have previously been used to infer past westerly wind variability. Here we present new diatom data from 52 lakes to assess diatom–environment relationships and develop an updated diatom–conductivity model for Macquarie Island. Seasonal and multi-year water chemistry and isotope data were analysed to assess temporal variability in hydrochemical processes and the influence of evaporation, ensuring the resulting diatom-conductivity model reflects external climatic drivers rather than local dynamics. Statistically robust transfer functions were developed for EC (bootstrapped $r^2 = 0.80$, RMSEP = 0.40), while pH and temperature had weaker predictive performance. For EC, weighted averaging and maximum-likelihood approaches performed comparably, although the former showed reduced predictive power at high EC where low species turnover and nutrient collinearity affected accuracy. This quantitative-diatom model combined with understanding of hydrogeochemical processes provides an improved basis for reconstructing past Southern Hemisphere westerly wind variability, which can be applied in future palaeoclimate studies on Macquarie Island.

1 Introduction

The Southern Ocean region exerts a strong influence on Southern Hemisphere and global climates (Jones et al. 2016; Fogt and Marshall 2020). Sub-Antarctic islands are among the few landmasses located in the Southern Ocean, making them important sites for understanding the past and future role of the Southern Ocean on climate variability. The Southern Hemisphere wwesterly winds (SHW) are a major driver of Southern Hemisphere mid- to high-latitude climates, modulating ocean circulation, mid-latitude temperature and precipitation regimes, and the efficiency of the Southern Ocean carbon sink (Gillett et al. 2006; Le Quéré et al. 2009; Fletcher et al. 2021; Menviel et al. 2023; Thomas et al. 2025). Instrumental data show that in recent decades the SHW have intensified and shifted poleward in response to warming (Marshall 2003; Fogt and Marshall 2020). These changes have been linked to an increase in net outgassing of carbon dioxide (CO_2) from deep-storage reservoirs in the Southern Ocean, with significant implications for future atmospheric CO_2 levels and global temperatures (Goyal et al. 2021; Nicholson et al. 2022; Mongwe et al. 2024; Olivier and Haumann 2025). Understanding long-term SHW variability is key to assessing the impacts of SHW dynamics under future climate warming scenarios.

Diatoms are highly sensitive to environmental changes and are widely used as palaeolimnological proxies in palaeolimnology to infer climate and environmental changes (Roberts et al. 2000; Verleyen et al. 2004; Sterken et al. 2008; Recasens et al. 2015; Liao et al. 2020; Peng et al. 2022; Deng et al. 2025). Diatoms are well established as indicators of salinity and ionic composition, forming the basis of numerous diatom–salinity or -conductivity transfer functions across a range of environments (Gasse et al. 1997; Verleyen et al. 2003; Volik et al. 2017; Maslennikova 2020; Farqan et al. 2025). These approaches have been successfully applied in diverse settings demonstrating the reliability of diatom assemblages for reconstructing past hydrochemical and environmental change.

Previous work on sub-Antarctic Islands has demonstrated that aquatic diatom communities are significantly influenced by changes in salinity (inferred from electrical conductivity, (EC)), allowing quantitative diatom-conductivity models to be developed (Gremmen et al. 2007; Saunders et al. 2009; 2015; 2018; Perren et al. 2020; Van Nieuwenhuyze 2020; Perren et al. 2025). On sub-Antarctic islands, lake water salinity changes are largely controlled by wind-driven sea spray aerosol (SSA) inputs, via both wet and dry deposition, with increased inputs occurring when winds are stronger and vice versa (Evans

1970; Buckney and Tyler 1974; Saunders et al. 2009; 2015; Humphries et al. 2021). Based on this, diatom-conductivity transfer functions have been used to infer past Holocene SHW intensity on Macquarie Island (Saunders et al., 2018), ~~and~~ Marion Island (Perren et al. 2020) and in southern South America (Perren et al. 2025). These relationships are understood to reflect longer-term, integrated hydrogeochemical and ecological responses to persistent wind-driven sea-spray inputs, rather than event-scale meteorological forcing.

Earlier studies on Macquarie Island have analysed diatom-environment relationships (McBride 2009; Saunders et al. 2009) and their application as palaeoenvironmental and climate proxies (Keenan 1995; Saunders et al. 2013; 2018; Deng et al. 2025). However, from the late 1900s to early 2000's overgrazing from increasing invasive rabbit populations (~~108,000~~ up to 150,000 individuals estimated from 2005-2006) resulted in widespread ecosystem degradation, including erosion, vegetation loss, and altered organic inputs into lakes (Scott and Kirkpatrick 2008; Terauds 2009). This affected aquatic ecosystems and diatom diversity (Marchant et al. 2011; Saunders et al. 2013). The Macquarie Island Pest Eradication Programme successfully eradicated all invasive vertebrates (principally rabbits) from the island in 2011, triggering substantial ecosystem recovery (Springer, 2018; Fitzgerald et al., 2021). Although direct limnological data to assess ecosystem recovery of individual lakes is not available, widespread vegetation recovery following early efforts of the eradication programme in 2010-2011 provides strong evidence that ecosystem processes across the island are no longer characterised by extreme disturbance (Shaw et al. 2011; Springer 2018; Fitzgerald et al. 2021). This is expected to have decreased catchment erosion, and sediment and nutrient delivery into lakes relative to the peak disturbance period, resulting in post-eradication (recovering) ecosystems.

Reassessing diatom–environment relationships under current post-eradication ~~(recovery)~~ conditions is necessary, because earlier studies were conducted during a period of vertebrate-induced disturbance rather than under near-natural conditions ~~were conducted during a period of disturbance related to introduced invasive vertebrates rather than when the island was in a natural state~~ (Saunders et al., 2013). Developing new diatom models based on ~~recovered~~ post-eradication conditions may better represent pre-invasion baseline communities, improving the accuracy and ecological relevance of palaeolimnological reconstructions. Furthermore, incorporating revised taxonomy and newly identified species will enhance the model's ecological resolution and predictive performance.

Understanding the processes that drive lake water chemistry, such as precipitation, evaporation, groundwater inputs, and nutrient cycling, and how they vary across temporal and spatial scales is essential when interpreting diatom–environmental relationships. Meredith et al. (2022) defined hHydrogeochemical ~~analyses of lakes~~lake processes across Macquarie Island ~~,~~ showing that dominant processes vary locally, and lakes can be classified as predominantly influenced by SSAs, catchment processes (i.e., with greater water-rock interaction), or precipitation (i.e., more dilute lake waters) ~~(Meredith et al., 2022)~~. Sea-spray-influenced lakes occur near the west coast and on the western edge on the Macquarie Island plateau, where exposure to the SHW is greatest. In contrast, catchment-influenced lakes with higher terrestrial ion concentrations are found at lower elevations, and rainfall-influenced lakes with low ion concentrations occur at higher elevations. This hydrogeochemical ~~understanding~~ framework supports the hypothesis that for lakes near the west coast, including those on the western edge of the plateau, EC-related diatom variation on Macquarie Island primarily reflects SHW-driven sea-spray inputs rather than local hydrological or geochemical controls.

While present day ~~these~~ water chemistry p~~data p~~rovides valuable insight into spatial variability, it is necessary to quantify temporal variability in hydrogeochemical processes, particularly evaporation, to assess how seasonal, interannual, and longer-term changes modify ion concentrations in lakes, including those derived from SSA. Establishing seasonal and multi-year lake water hydrogeochemical datasets will enhance confidence in proxy interpretations and form a foundation for long-term monitoring of Macquarie Island lakes. Such ~~research is rare worldwide, and has~~ research is rarely applied to develop ecological transfer functions particularly in such remote, isolated settings, and has not yet been undertaken on other sub-Antarctic ~~i~~islands. ~~,~~ ~~M~~making These factors highlight the ~~This makes this study~~ importance of this work~~t~~ for understanding how sub-Antarctic Island ecosystems will respond to future climate and environmental changes, particularly given the rapid ~~which are experiencing rapid climatic and~~ ecological shifts in response to climate that are already documented across the region (le Roux and McGeoch 2008; Lee and Chown 2016; Nel et al. 2023).

Here, we present new data from lakes on Macquarie Island quantifying post-pest eradication relationships between surface-sediment diatom communities and environmental conditions. Using comprehensive water chemistry datasets from 2018 and 2022–23, we examine seasonal and interannual

variability to develop updated diatom–environment transfer functions. This integrated approach strengthens the application of diatom-based proxies and provides a first step towards long-term monitoring of sub-Antarctic lake systems by contributing to baseline ~~understanding~~ data and establishing an analytical framework ~~for tracking~~to track ecological and biogeochemical change. These transfer functions will be applied in future studies to reconstruct past Holocene climate variability on Macquarie Island.~~.~~

2 Methods and Materials

2.1 Study area: Macquarie Island

Macquarie Island (54°50'S, 158°85'E) is a small sub-Antarctic island (128 km^2) located in the Southern Ocean just north of the polar front, 1200 km south-west of New Zealand and 1300 km from the Antarctic continent (Fig. 1~~a~~). It is one of the few landmasses within the Polar Frontal Zone and modern core SHW belt (50–55°S; Fig.1), making it ideally suited to study past and current changes in the SHW, temperature, ~~the SHW,~~ and precipitation. It has a harsh, cool, wet, oceanic climate with low seasonality and high wind velocities throughout the year. Together, these represent the influence the SHW have on climate in the region~~representative of the core SHW belt , with low seasonality and high wind velocities~~ (Selkirk et al. 1990). The SHW prevail almost exclusively from the west and north-west with a mean annual wind speed of 35 km ~~/~~h^{-1} and gusts reaching 185 km h^{-1} ~~km/h~~ (between 1948-2025; BOM 2025). The continual dominance of the SHW drive environmental and ecosystems responses on a west-to-east gradient across the island (Chau et al. 2019; Meredith et al. 2022), including the deposition and accumulation of wind-blown inputs such as sea spray and minerogenic aerosols (Buckney and Tyler 1974; Saunders et al. 2009). Mean annual temperature ranges from 3.1–6.6°C, and the island experiences high annual rainfall of >~~-~~1000 mm with >~~-~~317 rainy days yr^{-1} (between 1948–2025; BOM 2025). Rainfall has increased in recent decades with a higher frequency of intense rainfall events, mostly occurring during winter, which are then accompanied by drier, windier summers (Andersen et al. 2009; Kong et al. 2025). Persistent cloud cover over the island results in low light levels and sunshine hours per day (average 2.4 h from 1948–2022; BOM, 2025).

Macquarie Island is geologically unique, being the only location worldwide where an intact marine ophiolite sequence of oceanic crust and upper mantle is exposed above sea level (Davis, 1987). The

island is composed mostly of pillow basalts with interspersed flows of massive basalt (Selkirk et al. 1990). Dolerite, ultrabasics and intrusives are also present but are confined to the northern third of the island (Mawson 1943). As widespread glaciation did not occur during the ~~global~~ Last Glacial Maximum (26–20 ka), marine, periglacial and subaerial erosional, rather than glacial processes, shaped the island as well as lake formation and ontogeny. The island is fringed by a low coastal terrace leading to steep-sided slopes (20–40°) that rise to form the island plateau sitting at ~200–400 m asl (Selkirk et al. 1990; McBride and Selkirk 1998).

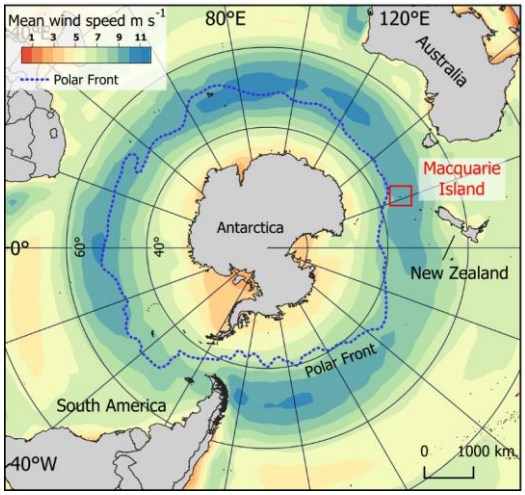

Fig~~ure~~ 1: Location of Macquarie Island in the Southern Ocean ~~relative to~~and mean annual wind speeds ~~-~~around the Southern Hemisphere (ERA5 reanalysis data 1960-2025), showing that the island lies within the ~~and~~ modern core ~~S~~Southern Hemisphere westerly wind~~W~~ belt (50–55°S~~°~~) ~~with mean wind speed shown.~~.

~~**Macquarie Island is geologically unique, being the only location worldwide where an intact marine ophiolite sequence of oceanic crust and upper mantle is exposed above sea level (Davis, 1987). The island is composed mostly of pillow basalts with interspersed flows of massive basalt (Selkirk et al. 1990). Dolerite, ultrabasics and intrusives are also present but are confined to the northern third of the island (Mawson 1943). As widespread glaciation did not occur during the global Last Glacial Maximum (26–20 ka), marine, periglacial and subaerial erosional, rather than glacial processes, shaped the island as well as lake formation and ontogeny. The island is fringed**~~

~~by a low coastal terrace leading to steep-sided slopes (20–40°) that rise to form the island plateau sitting at ~200–400 m asl (Selkirk et al. 1990; McBride and Selkirk 1998).~~

The island has numerous shallow and deep lakes and ponds across the plateau and coastal terrace (Fig. 2). High accumulation of surface water and a high water-table at or very near the surface lead to the formation of extensive mires across the island (Löffler 1984). While lake edges can form thick ice cover during winter, complete freezing of the lakes is not typically observed (Evans 1970; Selkirk-Bell and Selkirk 2013). The island is vegetated by bryophytes, tussock grass, herbs and sedges, with no shrub or tree species present (Selkirk et al. 1990).

2.2 Data collection

Surface sediments and water samples were collected from lakes on Macquarie Island during the 2022–23 austral summer (referred to as 2022). Sites were selected to replicate those sampled in 2018 that were published by Meredith et al. (2022).

Lake surface sediments were collected from 30 plateau (inland) sites for diatom analyses (lake ID = LK), representing conditions more than 10 years post-rabbit and rodent eradication. Surface sediments (top 2 cm) were collected from each site using a long-handled scoop from <1.5 m water depth. This method for sediment collection was selected for its logistical feasibility. Sediment mixing was minimised by visually assessing sampling depth and subsampling where necessary to retain only the upper ~2 cm. Sediments were generally well consolidated and remained intact during collection. Based on available lead-210 (^{210}Pb) chronologies from Macquarie Island lake cores, this interval represents approximately 10 years of accumulation (Saunders et al. 2013; Saunders et al. 2018), comparable to surface sediment sampling approaches used in previous studies (e.g. Saunders et al., 2009). An additional 17 coastal and five plateau sites sampled in 2006 (lake ID = S; Saunders et al. 2009) were included in the diatom dataset to extend the EC and nutrient gradients of the updated dataset, totalling 52 samples (Fig. 2a). Two lakes were replicated in the 2006 and 2022 seasons (S9 = LK40, S18 = LK2; Fig. 2a).

Lake water general parameters were measured in-situ at each site, including temperature, EC, dissolved oxygen (DO), and pH using a YSI ProQuatro Multiparameter Meter, with calibration performed prior to every sampling trip. DO was calibrated in water-saturated air following YSI manufacturer protocols.

Conductivity was calibrated using a 1413 µS cm^{-1} standard solution, and pH was calibrated using a three-point procedure with pH 4.0, 7.0, and 10.0 buffer solutions. Water samples were collected at all diatom sampling sites to measure total oxidised nitrogen (TON), phosphate (PO_4^{3-}), and silica (Si). Additional water samples were collected from 40 plateau sites for water chemistry analysis (Fig. 2b), including major ions and stable water isotopes (oxygen [($\delta^{18}O$)] and hydrogen [(~~$\delta^{2}H$~~)]). Each site was sampled three times across the 2022–23 season (November, December to January, and February). All water samples were collected from ~20 cm below the water surface and were filtered in-situ with 0.45 µm polyethersulpone filters into High Density Poly-Ethylene (HDPE) bottles following the method described by Meredith et al. (2009)). Water samples were refrigerated (4°C) until analysis.

Major ions, and oxygen ($\delta^{18}O$) and hydrogen ($\delta^{-2}H$) stable isotopes were analysed at the Australian Nuclear Science and Technology Organisation (ANSTO). Cations and anions were analysed using inductively coupled plasma-atomic emission spectrometry (ICP-AES). $\delta^{18}O$ and $\delta^{-2}H$ stable isotopes were analysed with a Picarro L2130-i Cavity Ring-Down Spectrometer. Values were reported as per mill

(‰) deviations relative to the international standard V-SMOW (Vienna Standard Mean Ocean Water), with a reproducible precision of ±0.2 and ± 1.0‰, respectively.

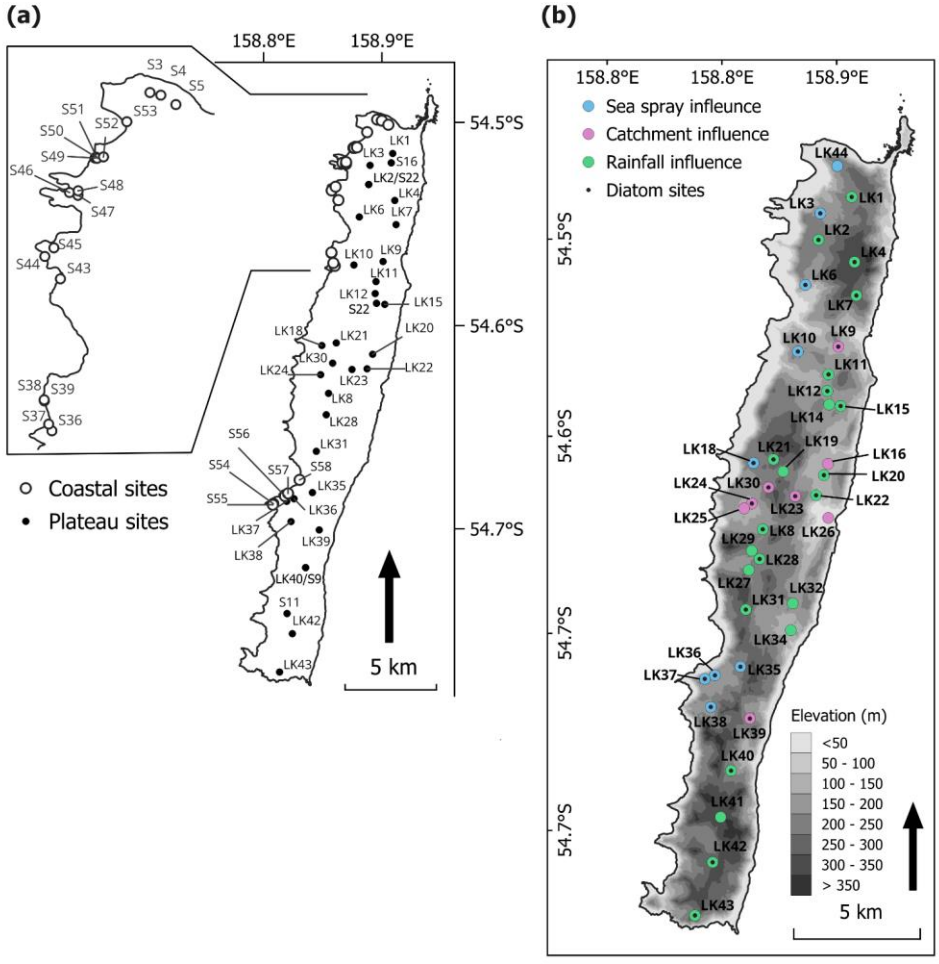

Fig~~ure~~ 2: Maps showing lake sites across Macquarie Island, **a)** Diatom surface sediment sites (coastal sites were originally sampled by Saunders et al. (2009); **b)** Lake water chemistry sites. Colours show lake types, based on dominate

hydrogeochemical processes, identified by Meredith et al., (2022). Black dots indicate that the site is also included in the diatom dataset.

Nutrient data from 2006 samples (filtered at 0.45µm) measured soluble reactive phosphate (SRP), TON (nitrate [(]NO_3[)] + nitrite [(]NO_2[)]), and silicate (Si) using an Alpkem Autoanalyser (Continuous Flow Solution Analyser), representing the operationally defined dissolved inorganic (and therefore readily bioavailable) fractions of total N, P, and Si. In contrast, the 2022 dataset measured TON, PO_4^{3-}, and Si ions using ICP-AES at ANSTO on filtered, undigested waters, with results reported as the corresponding inorganic species and concentrations consistently at or near detection limits. Despite methodological differences, the two approaches yield consistently low and broadly comparable concentrations in the two replicate lakes across sampling trips: for S9/LK40, PO_4^{3-} concentrations were 0.002 mg L^{-1} (autoanalyser) and <-0.01 mg L^{-1} (ICP-AES), and TON concentrations were 0.006 mg L^{-1} (autoanalyser) and <-0.06 mg L^{-1} (ICP-AES); for S18/LK2, PO_4^{3-} concentrations were 0.004 mg L^{-1} (autoanalyser) and <-0.01 mg L^{-1} (ICP-AES), and TON concentrations were 0.005 mg L^{-1} (autoanalyser) and < 0.06 mg L^{-1} (ICP-AES). Furthermore, if the 2022 analyses targeted the same reactive fractions measured in 2006, the results would still fall below or close to detection limits.

2.3 Diatom preparation and identification

Diatom preparation followed methods described by McBride (2009)[)]. Cleaned diatom solutions were mounted onto slides using Norland Optical Adhesive 61. At least 300–400 frustules were counted per sample, using Differential Interference Contrast (DIC) and oil immersion at 1000x magnification on a Zeiss Axioskope microscope, mounted with a TOUPTEK camera (U3CMOS). Species identification was primarily based on sub-Antarctic taxonomy described in Van de Vijer et al. (2002); Sterken et al. (2015); Sabbe et al. (2019); and Van de Vijver (2019). ~~Van de Vijer et al. (2002); Sterken et al. (2015); Sabbe et al. (2019); and Van de Vijver (2019)).~~ Species were photographed and documented (see Supplementary Material for an illustrated species catalogue).

2.4 Statistical analyses

2.4.1 Water chemistry

The lake water chemistry dataset was comprised of *in-situ* general parameters, major ion concentrations and $\delta^{18}O$ and $\delta^{2}H$ values from 2018 (Meredith et al. 2022) and 2022 (this study) to understand temporal

variation across the island. Data from 2018 (January to February) are referred to as sampling event 1 (E1) and sampling from the 2022 season as E2 (November), E3 (December to January), and E4 (February). Shapiro–Wilk tests showed that isotope data were normally distributed (p >0.05), whereas general parameters and ion concentrations deviated significantly from normality (p <0.05). Consequently, parametric tests (ANOVA, t-test, Tukey's HSD) were applied to normally distributed isotope data, and non-parametric tests (Kruskal–Wallis, pairwise Wilcoxon) to non-normally distributed general parameters ion data. A Principal Component Analysis (PCA) with z-score standardised data was performed to explore relationships between variables and assess the consistency of lake types identified by Meredith et al., (2022; Fig. 2b).

2.4.2 Diatom model

Diatom inference models were developed using diatom and environmental data collected from 2006 and 2022. Ordination methods were used to describe variation in the diatom dataset, explore diatom-environment relationships, and identify unique variance explained by environmental variables. Environmental variables included were EC, temperature, DO, pH, TON, PO_4^{3-}, and Si, with mean 2022 values used. Aadditional major ions were not included as these data were not available for 2006 sites. Water depth was not included as a variable as all sediment samples were collected within a narrow range samplingof 0–1.5 m water depth, rendering ecological changes in depth negligible. Additionally, water depth is often regarded as a composite variable that acts as a surrogate for complex environmental gradients (e.g., habitat type, light, salinity, nutrients, oxygen, and taphonomy) that are largely unknown and unquantified, and therefore its inclusion can lead to spurious and misleading results (Birks et al. 1998; Juggins 2013). Weighted Averaging (WA) was applied to dominant species to determine species ecological optima and tolerance. Together WA, Weighted Averaging Partial Least Squares (WAPLS), and Maximum Likelihood (ML) models were used to develop diatom transfer functions, with cross-validation used to assess model robustness.

The relative abundance of each diatom species in each sample was calculated as the percentage of the total number of frustules counted per sample. Species occurring at ≤1% relative abundance were excluded from the dataset. A full species list can be found in Supplementary Material. Nutrient values that were below the limit of detection were substituted with the respective detection limit value (PO_4^{3-}, =

0.01 mg L^{-1}, Si = 0.1 mg L^{-1}, TON = 0.06 mg L^{-1}). Environmental variables were screened for skewness, with temperature, EC, PO_4^{3-}, Si, and TON log(x+1) transformed.

PCA was performed on transformed environmental data to identify the primary gradients of environmental variation across sites. Detrended Correspondence Analysis (DCA) with detrending by segments and ~~downweighting~~downweighting of rare species was performed on untransformed species data to determine whether species distributions were linear or unimodal. As the DCA axis 1 gradient length (8.2 deviation units) was > 4, unimodal ordination methods were deemed appropriate (Ter Braak and Prentice 1988). Species data were log(x+1) transformed for remaining analysis.

A series of Canonical Correspondence Analyses (CCA) were then performed with forward selection, and scaling focused on inter-species distances, biplot scaling and downweighting of rare species. Variance Inflation Factors (VIF) of environmental variables were used to assess collinearity. As no variables had a VIF >10, none were excluded. A full CCA, with all environmental variables included, was first performed to quantify the total amount of species–environment variance~~iation~~ explained by the full set of variables. A series of independent and partial CCAs with variance partitioning were performed to constrain analyses, assess the relative explanatory power, and assess the unique and shared variance contributions of each variable. Individual CCAs, of each variable alone, estimate the marginal (unconstrained) explanatory power (i.e., how much variation a single variable explains when considered alone, without accounting for correlations with other variables). Partial CCAs assess the unique (conditional) contribution of each environmental variable after statistically controlling for all remaining variables. This analysis isolates the variance uniquely attributable to each predictor and identifies variables whose explanatory power is driven by covariation with others. Finally, variance partitioning was used to decompose the total explained variation into unique and shared fractions, allowing assessment of how much variation was due to individual predictors versus overlapping environmental gradients. Permutation test results (p > 0.05), CCA coefficients and lambda ratios (λ_1/~~–~~λ_2) of the first constrained eigenvalue (λ_1) to the second unconstrained eigenvalue (λ_2) were used to identify the environmental variables most appropriate for quantitative inference models. As a guide, high λ_1/~~-~~λ_2 ratios are necessary for a variable to have enough explanatory power to be included in quantitative inference models (Ter Braak and Prentice 1988; Juggins 2013). All ordination analyses were performed using the *vegan* package version 2.7-1 (Oksanen et al. 2013) in R (R Core Team, 2024).

ML and iterations of inverse ($_{INV}$) and classical ($_{CLA}$) WA models with and without tolerance downweighing, and WAPLS with up to five components were assessed to ~~provide~~ determine the best performing transfer functions. These methods were applied because they capture different aspects of species–environment relationships: WA provides a simple unimodal estimator; WAPLS allows more complex responses through latent components; and ML emphasises taxa with narrow ecological tolerances. Using multiple approaches therefore offers complementary strengths and helps identify the most reliable and robust model through cross-validation. All models were performed with bootstrapping and 100 iterations. Model R~~²~~^{2}, bootstrapped ~~²~~R^2 (R~~²~~$^2_{boot}$), root mean square error (RMSE) and root mean square error of prediction (RMSEP) values were used to assess performance. RMSEP and R~~²~~$^2_{boot}$ performance was favoured over R~~²~~^{2} and RMSE. RMSEP between WAPLS components was also used to assess overfitting. WA and WAPLS-1 results are often similar as WAPLS is built upon on the same weighted-averaging framework as WA (ter Braak and Juggins 1993). When this was the case and WAPLS components did not improve performance, WA was favoured as ~~it is the simplest~~the most parsimonious model. Software program C2 version 1.8 (Juggins 2003) was used to develop all transfer functions.

3 Results

3.1 Lake water chemistry

~~Analysis~~ Analyses of 40 plateau lakes on Macquarie Island showed that lake water general parameters (EC, pH and DO), and nutrients, did not vary significantly (p >~~-~~0.01) across the 2022 sampling events (E2-4; Table 1). Temperature ~~was seen to vary~~varied, being significantly lower in E2 compared to E3 and E4 (p <0.01). Lakes were~~are~~ moderately~~slightly~~ acidic (pH 5.7) to ~~slightly~~ alkaline (pH 9.14). Mean EC ranged from 126–261 µS cm^{-1}, with a decrease in EC from west to east across the island. Lakes were~~are~~ oxic (DO = 8.64–12.61 mg L^{-1}) and oligotrophic, with PO_4^{3-} and TON concentrations under or close to detection limits (<~~-~~0.01–0.02 mg L^{-1} and <~~-~~0.06–0.1 mg L^{-1}, respectively). Similarly, comparison with data from plateau lakes sampled in 2018 ~~plateau lakes~~ showed no significant difference (p >0.01) across all lake water general parameters, excluding temperature, indicating generally stable conditions in plateau lakes across years. However, a comparison between plateau lakes measured in 2022 and coastal lakes in 2006 did show significant differences (p <~~-~~0.01). Coastal sites in 2006 were generally eutrophic with higher nutrient ranges (TON = 0.007–4.636 mg L^{-1} and PO_4^{3-} = 0.1–9.9 mg L^{-1}), and higher

EC (406–1482 µS cm^{-1}), while temperature, DO, pH, Si were not significantly different ($p > 0.01$) (Table 1; see Supplementary Table S1 and S2 for full results).

~~Major ion analysis of the 40 plateau lakes showed that, although dilute in concentration, Cl (1.1–3.7 mmol L^{-1}) and Na (0.9–2.6 mmol L^{-1}) dominate the ionic composition of all lake waters (Table 2; see Supplementary Table S3 for full cation and anion results). All lakes showed similar ionic ratios to seawater for SO_4, Cl, Mg, and Na, suggesting a marine origin. Seawater ionic ratios diverged for K, Ca and F for some lakes, while SiO_2 was higher in all lakes, suggesting additional sources for these ions. (Fig. 3).~~

~~e~~

Table 1: Summary ~~table~~ of lake water general parameters and nutrient data. Temp. = temperature, DO = dissolved oxygen, EC = electrical conductivity, Si = silicate, PO_4^{-3} = phosphate, TON = total oxidised nitrogen.

	Temp. (°C)	DO (mg L^{-1})	EC (µs cm^{-1})	pH	Si (mg L^{-1})	TON (mg L^{-1})	PO_4^{3-} (mg L^{-1})
2022							
Mean	8.7	11.59	188	7.03	0.648	0.06	0.00467
Min	6.4	8.69	135	5.65	0.100	0.06	0.00326
Max	16.1	12.95	267	9.15	4.333	0.10	0.02391
E1 mean (n=39)	7.6	12.47	188	7.02	0.767	0.06	0.00568
E2 mean (n=37)	9.1	11.94	197	7.03	0.611	0.06	0.00414
E3 mean (n=39)	9.6	10.48	177	7.05	0.515	0.06	0.00351
2018 (n=40)							
Mean	9.4	10.95	153	7.35	-	-	-
Min	6.8	8.56	101	5.99	-	-	-
Max	15.8	12.64	292	9.21	-	-	-
2006 (plateau) (n=5)							
Mean	6.4	11.59	192	6.92	0.047	0.00564	0.0070
Min	5.5	11.35	164	6.35	0.003	0.00004	0.0013
Max	7.4	11.80	224	7.46	0.092	0.02449	0.0155
2006 (coastal) (n=17)							
Mean	8.4	11.32	889	7.19	0.719	1.23331	1.124
Min	6.0	9.17	406	5.50	0.074	0.02430	0.007
Max	13.1	14.43	1482	8.13	2.706	9.89000	4.636

Major ion analysis of the 40 plateau lakes showed that, although dilute in concentration, Cl (1.1–3.7 mmol L^{-1}) and Na (0.9–2.6 mmol L^{-1}) dominate the ionic composition of all lake waters (Fig. 3; see Supplementary Table S3 for full cation and anion results). All lakes showed similar ionic ratios to seawater for SO_4, Cl, Mg, and Na, suggesting a marine origin. Seawater ionic ratios diverged for K, Ca and F for some lakes, while SiO_2 was higher in all lakes, suggesting additional sources for these ions. (Fig. 4).

Statistical analyses showed no significant (p >0.005) differences in major ion concentrations across 2022 sampling events (E2–4). Broader changes were detected between 2018 and 2022, with Cl, SO_4, Br, and

Mg all showing significantly higher mean concentrations (p <0.005) in 2018 compared to all 2022 sampling events (E2–4). Fe, Na, K, Ca, F, SiO_2, and Al did not significantly vary (p >0.005) between sampling events. All ions that show significant variation (p <0.005) have predominantly marine sources.

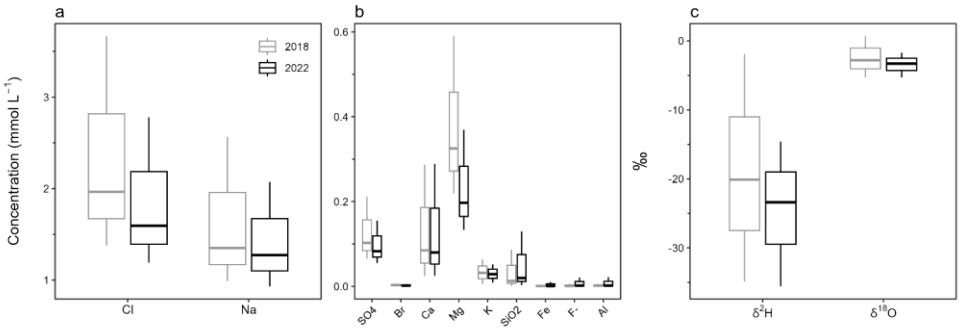

Fig. 3: Box and whisker plots showing the range and mean of 2018 and 2022 lake water major ions **a)** Cl and Na; **b)** SO_4, Br, Ca, Mg, K, SiO_2, Fe, F-, and Al; and **c)** stable water isotopes δ2H and δ18O.

~~Table 2: Mean major ions (mmol L^{-1}) and stable water isotope (‰) results for the 40 lakes sampled in 2018 and 2022.~~

	~~Cl~~	~~SO_4~~	~~Br~~	~~Na~~	~~Ca~~	~~Mg~~	~~K~~	~~SiO_2~~	~~Fe~~	~~F-~~	~~Al~~	~~δ^2H~~	~~$\delta^{18}O$~~
~~2018~~													
~~Mean~~	~~1.965~~	~~0.103~~	~~0.003~~	~~1.350~~	~~0.085~~	~~0.325~~	~~0.032~~	~~0.013~~	~~0.001~~	~~0.001~~	~~0.002~~	~~-20.1~~	~~-2.8~~
~~Min~~	~~1.379~~	~~0.065~~	~~0.001~~	~~0.987~~	~~0.025~~	~~0.219~~	~~0.005~~	~~0.001~~	~~0.000~~	~~0.001~~	~~0.000~~	~~-34.9~~	~~-5.3~~
~~Max~~	~~3.667~~	~~0.211~~	~~0.007~~	~~2.566~~	~~0.287~~	~~0.590~~	~~0.064~~	~~0.087~~	~~0.003~~	~~0.006~~	~~0.006~~	~~-1.9~~	~~0.7~~
~~2022~~													
~~Mean~~	~~1.593~~	~~0.083~~	~~0.002~~	~~1.272~~	~~0.080~~	~~0.197~~	~~0.029~~	~~0.020~~	~~0.001~~	~~0.002~~	~~0.002~~	~~-23.4~~	~~-3.3~~
~~Min~~	~~1.191~~	~~0.055~~	~~0.001~~	~~0.931~~	~~0.025~~	~~0.133~~	~~0.009~~	~~0.003~~	~~0.000~~	~~0.000~~	~~0.000~~	~~-35.6~~	~~-5.3~~
~~Max~~	~~2.779~~	~~0.155~~	~~0.005~~	~~2.073~~	~~0.289~~	~~0.369~~	~~0.052~~	~~0.130~~	~~0.011~~	~~0.021~~	~~0.022~~	~~-14.6~~	~~-1.7~~
~~E2 Mean~~	~~1.426~~	~~0.076~~	~~0.002~~	~~1.229~~	~~0.079~~	~~0.150~~	~~0.028~~	~~0.027~~	~~0.001~~	~~0.003~~	~~0.003~~	~~-30.1~~	~~-4.6~~
~~E3 Mean~~	~~1.436~~	~~0.075~~	~~0.002~~	~~1.228~~	~~0.081~~	~~0.150~~	~~0.027~~	~~0.022~~	~~0.001~~	~~0.002~~	~~0.002~~	~~-23.4~~	~~-3.2~~
~~E4 Mean~~	~~1.448~~	~~0.073~~	~~0.002~~	~~1.223~~	~~0.075~~	~~0.146~~	~~0.026~~	~~0.018~~	~~0.001~~	~~0.002~~	~~0.002~~	~~-20.7~~	~~-2.8~~

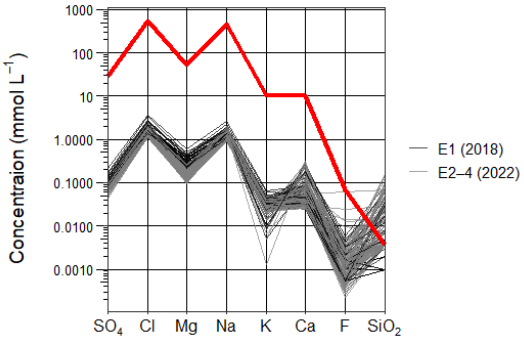

Fig.~~ure~~ 43: Scholler plot comparing the ionic composition (SO_4, Cl, Mg, Na, K, Ca, F and SiO_2) of Macquarie Island lake waters and seawater (red line), categorised into sampling years 2018 (black lines) and 2022 (grey lines).

~~Statistical analysis showed **almost** no significant differences in major ion concentrations across 2022 sampling events (E2–4), with the only significant difference occurring in Br between E2 and E4 (p = 0.023). Broader changes were detected between 2018 and 2022, with Cl, SO_4, Br, and Mg all showing higher mean concentrations in 2018 compared to all 2022 sampling events (E2–4). K and SiO_2 were greater in E1 in comparison to E4 and E2–3, respectively. Fe, Na, Ca, F, and Al did not significantly vary (p > 0.05) between sampling events. All ions that show significant variation (p <0.05) have predominantly marine sources.~~

PCA showed the relationship between lake water chemistry parameters, with samples grouped by lake type and sampling year (Fig. 54). Together, PC1 and PC2 captured 53% of the total variance in the dataset. PC1 represents a salinity and sea-spray gradient with variability in EC, distance from the west coast, Na, Cl, Br, Ca, Mg, and K captured. PC2 represents an altitude and terrestrial ion gradient with variability in elevation, temperature, SiO_2, Ca, Fe, and F captured. Lakes cluster according to environmental processes (groups derived from Meredith et al., 2022), with SSA influenced lakes having positive PC1 scores, which suggests higher concentrations of marine derived ions. ~~Three sea-spray influenced outliers can be seen across PC1: LK3 in 2018 and LK37 in both 2018 and 2022.~~ The grouping of samples influenced by catchment processes and those influenced by rainfall is driven by PC2 with catchment influenced~~unce~~ lakes having lower elevation and higher ion concentrations. SSA and rainfall

influenced lakes cluster based on the year that they were sampled with greater ion concentrations in 2018.

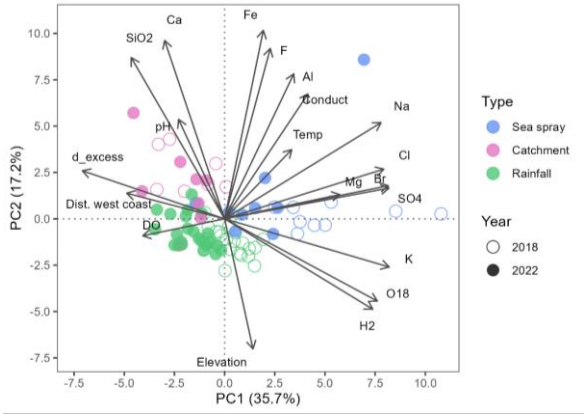

Fig.~~ure~~ 54: Principal Component Analysis (PCA) of Macquarie Island lake waters, showing the relationships between major ions and environmental parameters. Lakes are coloured by lake type, showing that lakes cluster based on the dominate geochemical processes identified by Meredith et al., (2022). Dist. west coast = distance from the west coast (m), Conduct = electrical conductivity.

3.2 Stable water isotopes

~~The~~ δ^2H and $\delta^{18}O$ ~~values~~ were measured in the 2022 samples and ranged from -38.3 to -9.2‰ and -38.3‰ to -0.67‰, respectively**.** Lake waters in 2018 and 2022 fell below the Global and Cape Grim (northwest Tasmania) Meteoric Water Lines (MWLs), suggesting slight isotopic enrichment in Macquarie Island's lakes (Fig. 6~~5~~). In 2018, lake waters were significantly higher in δ^2H (mean -24.8 ‰) and $\delta^{18}O$ (mean -2.83‰) compared to 2022 (mean δ^2H = -24.8 ‰ and $\delta^{18}O$ = -3.55 ‰)**.** Significant isotopic enrichment of δ^2H and $\delta^{18}O$ (p < 0.001) can be seen in the data at the beginning of the 2022 austral summer (E2–3; Fig. 6~~5~~a). SSA influenced lakes tended to have higher isotopic values, while catchment influenced lakes had lower values (Fig. 6~~5~~b), with a significant difference between all lake types detected (p < 0.001). LK20 and LK21 from E2 were outliers, plotting above the MWLs with lower $\delta^{18}O$ values. Cl concentrations appeared to be related to δ^2H and $\delta^{18}O$ values (Fig. 6~~5~~c), however the correlation

between the parameters was low (R^2 ~~r^2~~ ≤ 0.24). This lack of relationship was consistent across lake types and sampling events.

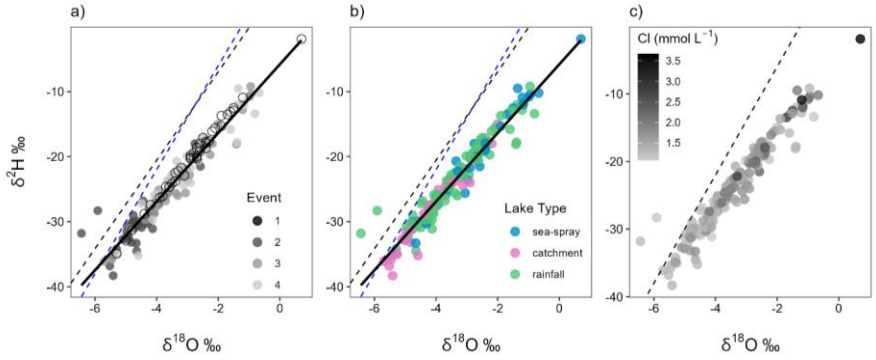

Fig~~ure~~ ~~6~~5: Stable water isotope δ^2H and $\delta^{18}O$ differences in Macquarie Island lake waters, shown across: ***a)*** sampling events; ***b)*** lake type; ***c)*** δ^2H and $\delta^{18}O$ relationship shown with Cl concentration (mmol L^{-1}). Solid black line shows Macquarie Island regression, blue dashed line is the Gglobal Mmeteoric Wwater Lline (GMWL: $\delta^2H = 8\ \delta^{18}O + 10$), and black dashed line is the Cape Grim Llocal Mmeteoric Wwater Lline (LMWL: $\delta^2H = 6.8\ \delta^{18}O + 6.65$).

3.3 Diatoms

3.3.1 Diatom communities

In total, 141 diatom taxa from 45 genera were identified in the 52 plateau and coastal lakes. Ninety-six taxa (including 21 unknown species) ~~-~~from 30 genera remained in the dataset after taxa with < 1% relative abundance were excluded. The most taxon-rich genera were *Pinnularia* (16 taxa), *Psammothidium* (12 taxa), and *Planothidum* (8 taxa). The most dominant taxa being both common, occurring in > 15 lakes, and abundant, occurring > 25% relative abundance in at least one sample, were *Aulacoseira principissa* Van de Vijver, *Psammothidium abundans* (Manguin) Bukhtiyarova & Round, *Psammothidium confusum* var. *atomoides* (Manguin) van de Vijver, unknown species 111, *Psammothidium confusum* (Manguin) van de Vijver, *Fragilaria capucina* Desmazières, and *Navicula bergstromiana* Vyverman et al. Coastal and plateau lakes ~~-~~showed distinctly different assemblages, with coastal lakes exhibiting less diversity (mean number of species = 20) and dominated by taxa including *F. capucina*, unknown sp. 111, *Planothidium quadripunctatum* (D.R.Oppenheim) Sabbe, *Planothidium delicatum* (Kützing) Round & Bukhtiyarova, and *Planothidium lanceolatum* (Brébisson ex Kützing) Lange-Bertalot. Plateau lakes were

Formatted: Font: 9 pt, Not Bold
Formatted: Font: 9 pt
Formatted: Font: 9 pt, Not Bold
Formatted: Font: 9 pt
Formatted: Font: 9 pt, Not Bold
Field Code Changed
Formatted: Font: 9 pt
Formatted: Font: 9 pt, Not Bold
Formatted: Font: 9 pt
Formatted: Font: 9 pt, Not Bold
Formatted: Font: 9 pt, Not Bold
Formatted: Font: Not Italic

more diverse (mean number of taxa = 40) and dominated by *A. principissa, P. abundans, P. confusum* var. *atomoides, P. confusum*, and *N. bergstromiana, Achnanthidium modestiformis* (Lange-Bertalot) Van de Vijver, *Cocconeis placentulata* Ehrenberg, and unknown species 2~~1~~1. ~~–~~No taxa were found in all lakes and none were uniquely restricted to either coastal or plateau lakes, although clear differences in species composition and relative abundance were observed. See Figure 7~~6~~ for microscopy photos of the most abundant taxa.

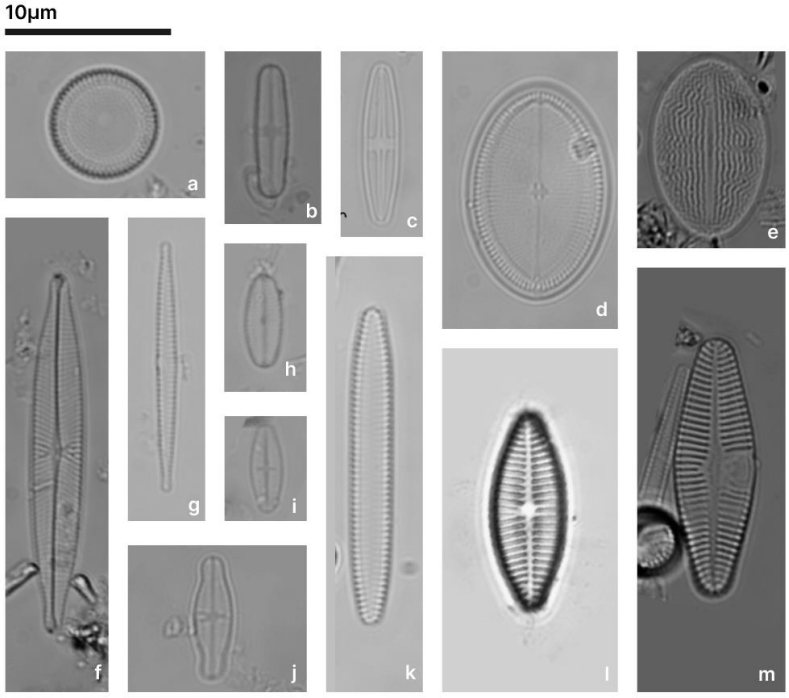

Fig.~~ure~~ 7~~6~~: The most abundant diatom taxa from plateau and coastal lakes on Macquarie Island. **a)** *Aulacoseira principissa*; **b)** *Psammothidium abundans*; **c)** *Psammothidium confusum*; **d-e)** *Cocconeis placentulata*; **f)** *Navicula bergstromiana*; **g)** *Fragilaria capucina*; **h)** Uunknown species 21; **i)** *Psammothidium confusum* var. *atomoides*; **j)** *Achnanthidium modestiformis*; **k)** Uunknown species 111; **l)** *Planothidium delicatulum*; **m)** *Planothidium lanceolatum.*

Formatted: Font: Not Italic
Formatted: Font: 9 pt, Not Bold
Formatted: Font: 9 pt
Formatted: Font: 9 pt, Not Bold
Formatted: Font: 9 pt
Formatted: Font: 9 pt, Not Bold
Formatted: Line spacing: 1.5 lines
Formatted: Font: 9 pt
Formatted: Font: 9 pt, Not Bold
Formatted: Font: 9 pt
Formatted: Font: 9 pt, Bold
Formatted: Font: 9 pt
Formatted: Font: 9 pt, Not Bold
Formatted: Font: 9 pt
Formatted: Font: 9 pt, Not Bold
Formatted: Font: 9 pt
Formatted: Font: 9 pt, Not Bold
Formatted: Font: 9 pt
Formatted: Font: 9 pt, Not Bold
Formatted: Font: 9 pt
Formatted: Font: 9 pt, Not Bold
Formatted: Font: 9 pt, Not Bold, Not Italic
Formatted: Font: 9 pt, Not Bold
Formatted: Font: 9 pt
Formatted: Font: 9 pt, Not Bold
Formatted: Font: 9 pt
Formatted: Font: 9 pt, Not Bold
Formatted: Font: 9 pt
Formatted: Font: 9 pt, Not Bold
Formatted: Font: 9 pt
Formatted: Font: 9 pt, Not Bold

3.3.2 Diatom-environment relationships

The full CCA model was significant (p = 0.001), with environmental variables explaining 23.9% (Table 2~~3~~) of the total variance in diatom species composition (constrained inertia = 1.5). Together, the first two canonical axes explained 62.8% of the total constrained variance (Table 2~~3~~; Fig. 8~~7~~). Forward selection with Bonferroni corrections, identified EC and ~~,~~ pH (p = 0.003), and temperature (p = 0.015) as the most significant predictors of diatom community composition ~~(p = 0.001)~~, collectively explaining 15.4 ~~-~~% of the total variance. This equates to 70% of the total explained variance in the full model, capturing the major environmental gradients influencing species distribution with a more parsimonious model.

Table 2~~3~~: Full CCA model results

Axis	Eigenvalue	Proportion of variance explained (%)	Cumulative proportion (%)
CCA1	0.77	51.07	51.07
CCA2	0.38	25.14	76.21
CCA3	0.22	14.55	90.76
CCA4	0.144	9.24	100.00
Constrained inertia	1.5		
Constrained proportion (%)	~~23.97~~19.57		

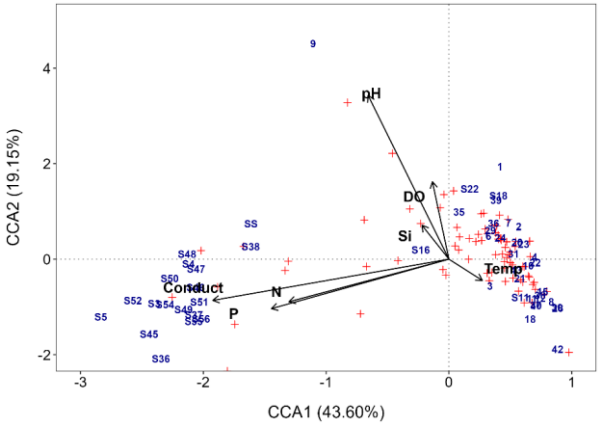

Fig~~ure~~ 8~~7~~: Full CCA ordination biplot of diatom species and environmental data, numbers indicate sites, and grey symbols indicate diatom species. Si = silicate, P = phosphate, N = total oxidised nitrogen, and conduct = electrical conductivity (EC).

Formatted: Not Highlight
Formatted: Not Highlight
Formatted: Not Highlight
Formatted: Font: Italic, Not Highlight
Formatted: Not Highlight
Formatted: Not Highlight
Formatted: Not Highlight
Formatted: Font: Italic, Not Highlight
Formatted: Font: Italic
Formatted: Not Highlight
Formatted: Not Highlight
Formatted: Font: 9 pt, Not Bold
Formatted: Font: 9 pt, Not Bold
Formatted: Font: 9 pt, Not Bold
Formatted: Font: 9 pt, Not Bold
Formatted: Line spacing: 1.5 lines
Formatted: Font: 9 pt
Formatted: Font: 9 pt, Not Bold

Individual CCAs were performed to assess the total explanatory power of each variable. EC and pH were shown to be the strongest, individually explaining 10.03% and 4.56% of the total variation, respectively. This corresponds to 45.83% and 20.86% of the total variance in the full CCA model. Additionally, EC was the only variable with a high λ_1/λ_2 ratio (λ_1/λ_2 = 1.31; Table 34), suggesting it is the only variable with enough explanatory power for inference modelling.

Table 34: Individual CCA results, independent CCAs run for each variable. (* = significant *p value* < 0.05)

Variable	λ_1 / λ_2	Constrained sum	Variance explained (%)	Proportion of full model explained (%)	p-value
Electrical conductivity	1.31	0.64	10.0362	45.8342.28	0.001*
Phosphate	0.73	0.4038	6.5902	27.526.23	0.001*
Total oxidised nitrogen	0.68	0.357	5.7886	26.7822.99	0.001*
pH	0.39	0.3329	5.434.56	20.8621.63	0.001*
Silicate	0.26	0.1920	3.142	14.6112.48	0.03423*
Temperature	0.22	0.147	2.2762	11.969.03	0.382176
Dissolved oxygen	0.12	0.120	1.9751	6.97.85	0.586879

Partial CCAs were performed with each environmental variable tested separately while controlling for covariation with all other variables, to quantify unique and shared variance contributions. EC, pH, and Si were the only variables to have significant unique contributions ($p \leq 0.01$; Table 4 Partial CCA Table 5). The shared and unique variance of each environmental variable is shown in Figure 98. EC explained the largest proportion of total constrained variation (46%) in diatom community composition, with a large shared component (17% unique, 28% shared), suggesting it acts along a major environmental gradient shared with TON and PO_4^{3-} (Fig. 8). Despite this, it performed well in all other CCAs and its unique contribution remained high, indicating it is an important independent driver of diatom structure across Macquarie Island lakes. Furthermore, low VIFs among all environmental variables (VIFs <3) indicated that multicollinearity was low. EC (VIF = 2.6) showed a low correlation with other variables ($R^2 \leq 0.47$), suggesting it represents a largely independent gradient in the dataset. In contrast, pH had similar unique variance (18.4%) and lower shared variance (2.4%), implying a more independent ecological influence.

Formatted: Font: 9 pt, Not Bold

Formatted: Font: 9 pt, Not Bold

Formatted: Font: 9 pt, Not Bold

Table 45: Partial CCA results, where each variable was tested with the covariation of other variables controlled (* = significant *p value* < 0.05).

Variable	Variance explained (%)	Proportion of full model explained (%)	p-value
pH	5.9702	18.9235	0.0012*
Electrical conductivity	5.584.85	17.627	0.001*
Silicate	3.875	13.9311.99	0.008*
Temperature	3.032.81	10.878.61	0.151
Total oxidised nitrogen	2.1406	6.287.6	0.651
Phosphate	1.718	6.375.20	0.774
Dissolved oxygen	1.346	4.068	0.991

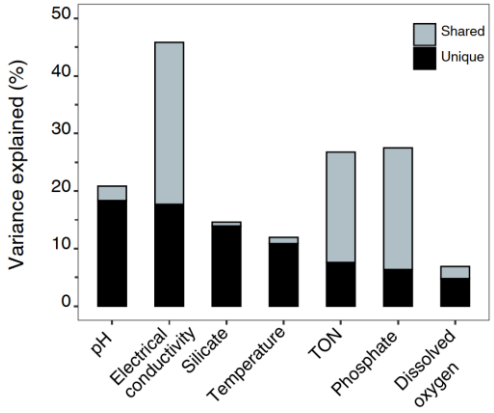

Fig. 98: Variance partitioning showing unique and shared proportions of variance explained by each environmental variable.

3.3.3 Species optima and tolerances

Species optima ~~and tolerance~~ across major environmental gradients EC and ~~,~~ pH~~, and temperature~~ were determined with WAA. *F. capucina, P. lancelotaum*, and *P. delicatulum* were found across the EC range with broad tolerances, however each species showed different optima (Fig. 109). The apparent bimodal distribution of *F. capucina* likely reflects ecological plasticity across differing hydrochemical conditions and/or potential taxonomic aggregation within this morphotype. Exploration of a GAM-based response curve (Fig. S2) indicates *F. capucina* has a weak non-linear relationship with EC, suggesting a broad

Formatted: Font: 9 pt, Not Bold
Formatted: Font: 9 pt, Not Bold
Formatted: Font: 9 pt, Not Bold
Formatted: Line spacing: 1.5 lines
Formatted: Font: 9 pt, Not Bold
Formatted: Font: 9 pt
Formatted: Font: Italic

and flexible ecological response rather than a strongly defined unimodal optimum. Unknown sp. 111 was found to tolerate ~~mid to~~ high ~~level~~ EC, while most other dominant species, including *A. principissa*, *C. placentulata*, *N. bergstromiana* and dominant *Psammothidium* species show~~have~~ tolerance and optima for ~~highest abundance at~~ low EC ~~sites~~.

~~Species optima were less clear for pH, as the~~ D~~d~~ominant diatom species ~~had tolerances~~occurred across the pH gradient, with species optima ranging from ~~slightly~~ moderately acidic to ~~slightly alkaline~~neutral (Fig. 1~~0~~). Most dominant species had optima for moderate acidity, with ~~*A. principissa*, *N. bergstormiana*, and~~ *Psammothidium* species, *A. principissa*, and *N. bergstormiana* showing narrow pH tolerances. *C. placentulata* and *F. capucina* ~~*confusum* var. *atomoides*~~ showed ~~optima for slightly acidic sites~~broader tolerances and ~~. While *P. confusum* had higher abundances at slightly alkaline sites. *C. placentulata*, *P. lanceolatum*, *P. quadripunctatum*, and unknown sp. 21 showed preferences for neutral pH, u~~and ~~u~~nknown sp. 111 ~~for neutral to slightly acidic sites.~~was the only dominant species with a near neutral optima. ~~Species optima for temperature are described in Supplementary Material Figure S1.~~

Formatted: Font: Not Italic

Formatted: Font: Not Italic

Formatted: Font: Not Italic

Formatted: Font: Not Italic

Formatted: Font: Italic

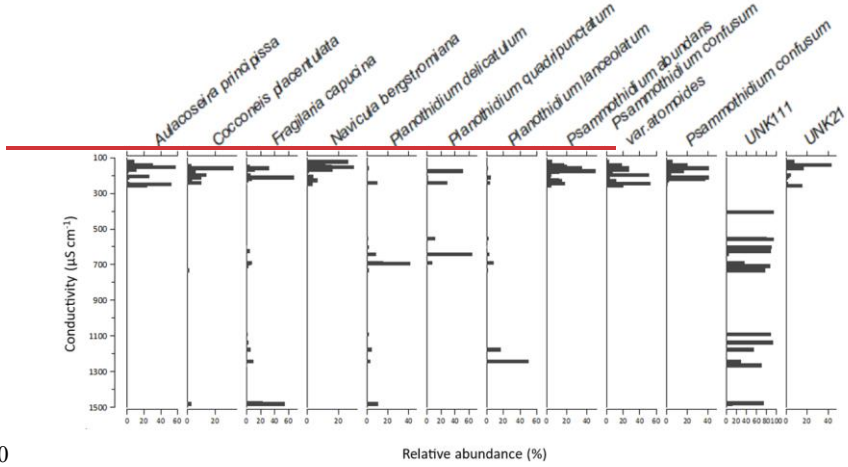
Aulacoseira principissa
Cocconeis placentulata
Fragilaria capucina
Navicula bergstromiana
Planothidium delicatulum
Planothidium quadripunctatum
Planothidium lanceolatum
Psammothidium abundans
Psammothidium confusum var.atomoides
Psammothidium confusum
UNK111
UNK21
Conductivity (µS cm-1)
100
300
500
700
900
1100
1300
1500
0 20 40 60
Relative abundance (%)

500

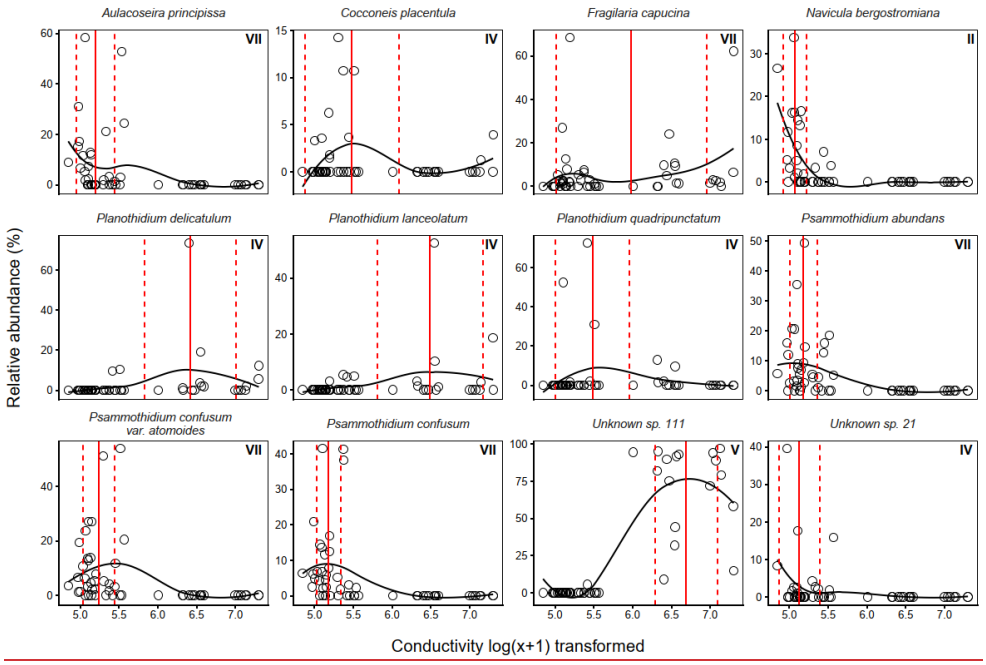

Fig~~ure~~ 109: Weighted averaging (WA) electrical conductivity optima (solid red line) and tolerance ranges (dashed red lines) for dominant diatom species from Macquarie Island lakes. Observed relative abundances (%) are plotted against log-transformed conductivity, with fitted loess curves illustrating species response shapes along the conductivity gradient (126–1482 µS/cm). Roman numerals indicate Gaussian response curve type. ~~Relative abundance of the most dominant diatom species along the conductivity gradient (126–1482 µS/cm), UNK = unknown species.~~

Formatted: Font: 9 pt, Not Bold

Formatted: Font: 9 pt

Formatted: Line spacing: 1.5 lines

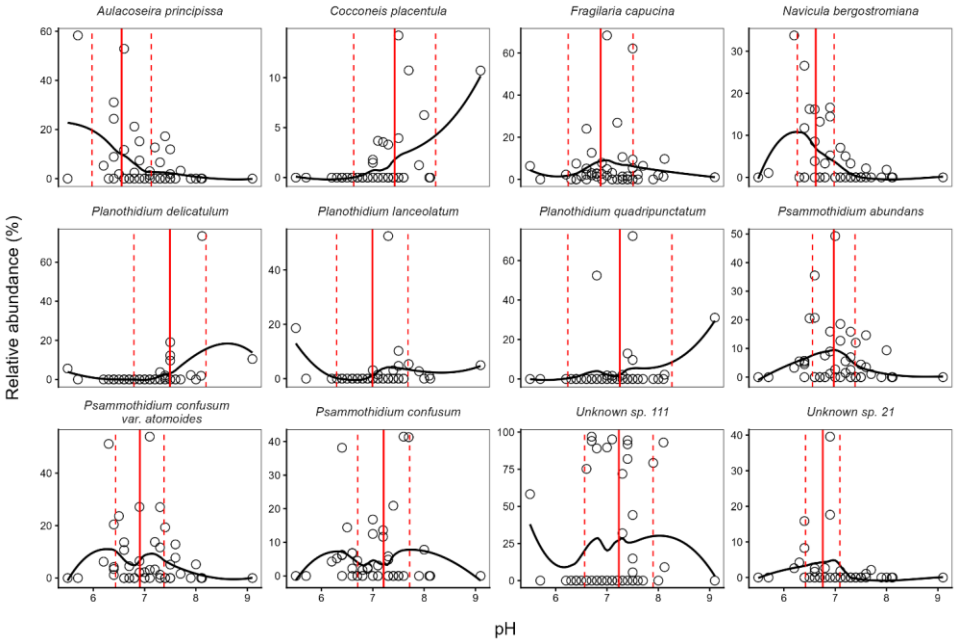

Fig. ~~ure~~ 1~~0~~: Weighted averaging (WA) pH optima (solid red line) and tolerance ranges (dashed red lines) for dominant diatom species from Macquarie Island lakes. Observed relative abundances (%) are plotted against **pH**, with fitted loess curves illustrating species response shapes along the pH gradient (5.50–9.14 °C). ~~**Relative abundance of the most dominant diatom species along the pH gradient (5.50–9.14 °C), UNK = unknown species.**~~

Formatted: Font: 9 pt, Not Bold

Formatted: Font: 9 pt, Not Bold

Formatted: Font: (Default) Times New Roman, 12 pt

Formatted: Normal

3.3.4 Diatom transfer functions

Ordination analyses showed that EC and pH explained significant and independent proportions of variance in diatom composition. While temperature also showed significant but lesser contributions, it was not considered for transfer function development as diatom-based temperature reconstructions as species responses to temperature can be indirect and influenced by multiple co-varying environmental gradients, limiting the reliability of temperature inference (e.g. Juggins, 2013). ~~, with temperature contributing to a lesser extent. As such, t~~ ransfer functions were developed for each. While Si was shown

to independently contribute to diatom variance, reduced CCA modelling with forward selection did not indicate it to be a major environmental gradient. Transfer functions were therefore only developed for EC and pH. Transfer function results for the best performing WA, WAPLS, or ML model for EC and pH~~each environmental variable~~ are described in Table 5~~6~~.

Table ~~5~~6: Best performing WA, WAPLS or ML model results for electrical conductivity and ~~,~~ pH~~, and temperature~~.

Variable	Model	R^2	R^2_{boot}	RMSE	RMSEP
Electrical conductivity	WA_{inv}	0.83	0.74	0.31	0.39
	ML	0.91	0.80	0.22	0.40
pH	WAPLS-2	0.72	0.26	0.34	0.60
		69	7		
~~Temperature~~	~~WAPLS-3~~	~~0.81~~	~~0.19~~	~~0.07~~	~~0.18~~

For EC, WA_{INV} and WAPLS-1 produced near identical results. WA_{INV} was favoured as the simpler model (WA_{INV}, R^2= 0.83, R^2_{boot}= 0.74, RMSE = 0.31, RMSEP = 0.39). Although WAPLS-2 to -5 increased R^2 and reduced RMSE, each successive component progressively increased RMSEP by 13-16%, thereby reducing performance. Given the unimodal gradient structure of the dataset, ML modelling was also assessed for EC. ML showed slightly stronger predictive performance to WA_{INV}, with higher R^2_{boot} and comparable RMSEP (ML, R^2= 0.91, R^2_{boot}= 0.80, RMSE = 0.23, RMSEP = 0.40).

Comparison of observed and predicted value scatter plots indicated that ML achieved a tighter fit, with WA_{INV} showing increased predictive error at higher EC ranges (Fig. 1~~2~~4). However, further inspection indicated that only ~30% of taxa displayed Gaussian (Type IV–V) response curves indicating ML may not be the most appropriate approach (Fig. 9 and see ~~see Supplementary Figure S2 and~~ Table S5~~4~~ for full Gaussian response curve results). However, overfitting from ML is not likely as RMSEP did not increase. Overall, both models show cross-validated performance and are considered robust.

pH had poor performance across all WA and WAPLS models with high RMSEP (≥ 0.6) and low R^2_{boot} (≤ 0.26). WAPLS-2 was found to be the strongest model (WAPL-2, R^2= 0.72, R^2_{boot}= 0.26, RMSE = 0.33, RMSEP = 0.60). ML modelling showed poor performance for pH with high RMSEP = 0.93.

Formatted: Font color: Auto

Formatted: Font: 9 pt, Not Bold

Formatted: Font: 9 pt, Not Bold

Formatted: Font: 9 pt, Not Bold

Formatted: Font: 9 pt, Not Bold

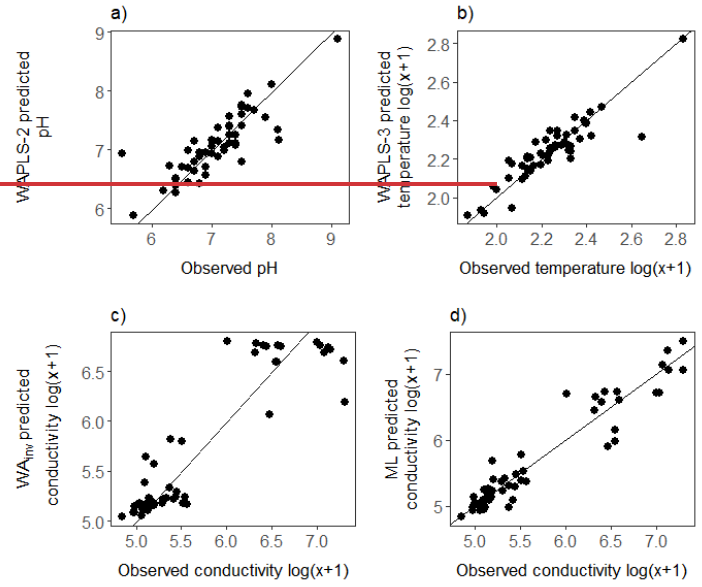

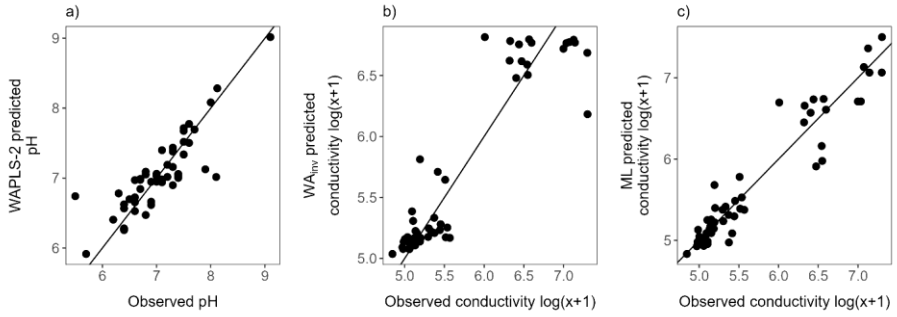

Fig. ~~ure~~ 1~~2~~4: Comparison of observed environmental measurements with values predicted by diatom-based transfer functions: **a)** pH estimated using WAPLS-2; **b)** ~~temperature estimated using WAPLS-3; c)~~ conductivity estimated using WA with inverse deshrinking (WA$_{INV}$); and ~~c~~**d)** conductivity estimated using the maximum likelihood (ML) method. Black lines show the 1:1 line.

Formatted: Font: Not Bold, Not Highlight

Formatted: Line spacing: 1.5 lines

Formatted: Not Highlight

Formatted: Font: Not Bold, Not Highlight

~~pH had poor performance across all WA and WAPLS models with high RMSEP (> 0.6) and low r^2_{boot} (≤ 0.2). WAPLS 2 was found to be the strongest model (WAPL 2, r^2 = 0.69, r^2_{boot} = 0.17, RMSE = 0.34, RMSEP = 0.63). Temperature had similarly low r^2_{boot} (< 1.9) across models but low RMSEP (≤ 0.2) with WAPLS 3 showing the best performance (WAPLS 3, r^2 = 0.81, r^2_{boot} = 0.19, RMSE = 0.07, RMSEP = 0.18). ML modelling showed poor performance for pH with high RMSEP = 0.93 and temperature with low r^2_{boot} = 0.08.~~

4 Discussion

4.1 Annual and seasonal lake water hydrogeochemical variation

The seasonal hydrochemistry dataset presented in this study support the 2018 baseline assessment (Meredith et al., 2022) that lake water chemistry is controlled by SSAs, terrestrial catchment processes, elevation and rainfall dilution.

The seasonal water chemistry data, which is presented for the first time in this study, shows that there is ~~little to~~ no significant variation in major ions across the 2022–23 austral summer. ~~Variations in Br were observed but can be explained as being related to localised sources associated with increased organic inputs from runoff rather than SSA sources. This is indicated by Cl/Br ratios generally falling below the seawater line (Supplementary Fig. S3), suggesting Br has additional non marine sources. Br is known to be enriched in dissolved and particulate organic matter and mobilised during catchment run-off events, particularly in peat-dominated sub-Antarctic landscapes~~ (Gerritse and George 1988; Biester et al. 2004; Guevara et al. 2019)~~. This interpretation is further supported by differing monthly rainfall amounts for Macquarie Island, where higher mean monthly rainfall occurred during E3 (January - 98 mm) and E4 (February -93 mm) compared to E2 (December -59 mm; BOM, 2025).~~

C~~A c~~omparison of 2018 and 2022 data shows that significant variation (p <~~-~~0.005), in some major ions is evident, with higher concentrations in 2018 of Br and Cl, SO_4, and Mg associated with SSAs. Although not statistically significant (p >~~-~~0.005), other sea-spray derived ion mean values (Na, Ca, K) were higher in 2018 (Fig. 3; Table S4~~Table 2~~).~~-~~ However, not all ions increased in concentration, ~~. In particular,~~ and

terrestrially derived ions such as Fe, F, Si, and Al were lower in 2018. This, suggestings that lakes in 2022 had a stronger SSA influence.

Despite these changes, PCA of the 2018 and 2022 lake water chemistry datasets (Fig. 54) show that lakes typically cluster by the lake types identified in Meredith et al. (2022) (i.e., as SSA, catchment and rainfall influenced). This indicates that the major hydrogeochemical processes influencing Macquarie Island lakes are consistent between years, with no major environmental shifts occurring in weathering and erosion of the island's geology, suggesting these processes are stable on an annual time scale. Identifying hydrogeochemical stability is important for identifying lake sites suitable for diatom–conductivity inference models. It also strengthens palaeoclimate interpretations by suggesting that local lake dynamics are relatively constant, supporting the hypothesis that in sea-spray dominated lakes, proxies primarily record externally forced changes driven by the SHW rather than internal hydrological or geochemical dynamics (Saunders et al. 2018; Perren et al. 2020). This further emphasises that water chemistry characteristics are critical to consider in site-selection, to develop reliable SHW reconstructions on Macquarie Island.

~~Furthermore, the development of the transfer function using field parameters collected across multiple sampling events increases confidence that the model reflects representative environmental conditions~~ (Goldenberg Vilar et al. 2018; Kennedy and Buckley 2021)~~. This repeated sampling approach is rarely possible when constructing diatom transfer functions, particularly in remote regions like the sub-Antarctic and Antarctic. While this adds robustness to the diatom model developed here, the data does not include winter measurements. The transfer functions could therefore be improved with year-round lake monitoring to capture the full range of environmental variability.~~

4.2 Evaporation

Interpreting environmental proxies as direct indicators of climate variability can be challenging, as multiple processes may produce similar signals (Molén 2024). When using diatom–conductivity models to infer past SHW variability, it is essential to consider how near surface evaporation has the potential to concentrate ions in surface waters and mimic the effects of other processes such as increasing lake water salinity from SSA deposition due to stronger winds. Although this study and previous studies (Evans 1970; Buckney and Tyler 1974; Meredith et al. 2022) have demonstrated that SHW-driven SSA

inputs are a dominant control on lake water chemistry on Macquarie Island, the role of evaporation in amplifying these signals remains unclear.

To explore this, we analysed δ^2H and $\delta^{18}O$ values from 2018 and across the 2022–23 Austral summer. Isotopic enrichment is evident across the 2022–23 season (Fig. 65a), ~~unsurprisingly~~ indicating a strengthening evaporative signal through summer. Lake stable water isotopes sampled in 2018 were significantly more enriched than the 2022 mean, as expected given that the 2018 samples were collected in late summer, when evaporative effects are strongest and cumulative due to warmer temperatures throughout summer. This is supported by lake water temperatures being significantly lower in early summer (E2) compared to late summer (E3 and E4; Table 1). Given Macquarie Island's persistently high cloud cover, humidity, and low sunshine hours (BOM, 2025), solar evaporation is likely limited and confined to the summer season. Evaporation can produce heavy-isotope enrichment and the residual lake water becomes progressively enriched in heaver isotopes (δ^2H and $\delta^{18}O$), moving away from the Global MWL (Gat 1996). Comparisons between E1 (2018) and E4 (2022), which were sampled at the same time of the year in January–February provide a valuable comparison of potential interannual variability in lake water chemistry and processes (Fig. 3, Table S4~~Table 2~~). These two sampling events show near identical mean isotopic composition (p >-0.~~05~~01; δ^2H = -20.7‰ and $\delta^{18}O$ = -2.8‰ in 2022, and δ^2H = -20.1‰ and $\delta^{18}O$ = -2.8‰ in 2018), suggesting broadly stable summer evaporative conditions between years. Furthermore, SSA influenced lakes on the plateau are in proximity to the west coast and have the greatest exposure to the SHW (Fig. 2b). These lakes have significantly higher isotopic enrichment (Fig. 5b), providing further evidence that wind is likely the primary driver of evaporation in plateau lake waters across Macquarie Island, particularly in lakes located on the west~~ern~~ coast, which may be most suitable for reconstructions of SHW dynamics (Saunders et al., 2018). As both wind-enhanced evaporation and wind-driven SSA transport and deposition contributes to the concentration of SSA ions in these lakes, both ion deposition and the concentration reflect a SHW signal.

Cl^- is a robust tracer of hydrogeochemical processes and, together with δ^2H and $\delta^{18}O$ values, can be used to better understand evaporation (Kirchner et al., 2010). While the isotopic enrichment observed generally indicates an evaporative signal, the absence of a correlation between Cl^- and δ^2H or $\delta^{18}O$ (Fig. 6c) suggests that isotopes are capturing short-term (summer) evaporation rather than sustained evaporative concentration sufficient to increase Cl^- concentration in the lake waters like those in

environments driven primarily by solar evaporation (Meredith et al. 2009). On Macquarie Island, wind-driven SSA deposition and rainfall dilution therefore likely remain the primary drivers of Cl^- variability. Consequently, EC in lake waters of Macquarie Island remains a robust proxy for interpreting variations in SHW strength.

4.3 Diatom communities

Diatom analysis showed that typical sub-Antarctic genera (Van de Vijver 2019; Goeyers et al. 2022), including *Psammothidum*, *Planothidium*, and *Fragilaria*, dominated lake diatom communities on Macquarie Island. Across 52 lakes, 141 taxa were identified, indicating intermediate species diversity relative to previous studies on the island which reported 102 (McBride, 2009) and 208 (Saunders et al., 2009) species. Consistent with these earlier studies we have demonstrated that diatoms on Macquarie Island exhibit clear and distinct ecological preferences. Combined with the pronounced environmental gradients among lakes, these species-environment relationships provide a strong basis for using diatoms as indicators of limnological conditions and environmental change.

Psammothidium species are characteristic of low EC sites (Van de Vijer et al. 2002), and while abundance and dominance of key *Psammothidium* species showed variation along the lower end of the EC gradient (Fig. 10), they dominated low EC sites. *N. bergstromiana* is considered endemic to Macquarie Island and was commonly found with dominant *Psammothidium* species at low EC sites, typically occurring where EC was <200 µS cm^{-1}, consistent with what has previously been reported (Sabbe et al. 2019). *A. principissa*, previously identified as *Aulacoseria distans* (Ehrenberg) Simonsen on Macquarie Island (McBride, 2009; Saunders et al., 2009), was also common at low EC (Fig. 10). This taxa is commonly found on sub-Antarctic Islands and is suggested to prefer very low conductance values <80 µS cm^{-1} (Van de Vijver 2012), while EC was not observed < 160 µS cm^{-1} in this dataset, *A. principissa* may be an indicator of very low EC conditions.

P. lanceolatum was a dominant high EC, high nutrient taxa. While it has been found to dominate flora elsewhere, this contrasts previous studies where it has been reported to be characteristic of oligotrophic conditions (Van de Vijer et al. 2002). *F. capucina, P. delicatulum*, and unknown sp. 111 were more commonly dominant at high EC. *F. capucina* was found across the EC gradient displaying a bimodal

distribution (Fig. 10), consistent with its cosmopolitan and ecologically tolerant nature (Van de Vijer et al., 2002).

4.4 Developing transfer functions

A key aim of this study was to update and improve existing quantitative diatom models for Macquarie Island. While the dominant taxa identified here are consistent with those reported by Saunders et al. (2009), the strength of some diatom–environment relationships differ. EC and pH remain strong explanatory variables for diatom variation, whereas PO_4^{3-} and Si showed limited influence in ~~this~~the present study ~~study~~(Table 3 and 4)~~.~~. This reduced explanatory power likely reflects the low nutrient variability across plateau lakes, where concentrations were generally below detection limits.

Sub-Antarctic lakes are characteristically oligotrophic; high nutrient levels do occur, but they are associated with peatlands or animal colonies, as is the case with coastal lakes on Macquarie Island (Selkirk et al. 1990). ~~The~~ Saunders et al. (2009) ~~dataset~~ recorded greater nutrient variability across plateau sites at the lower end of the EC gradient, attributed to enhanced organic inputs during periods of high ecological disturbance from invasive rabbits. These differences suggest that the dataset in ~~this~~ the present study ~~better~~ represents post-eradication~~invasive~~ ~~or recovered~~ limnological conditions that ~~more likely~~are more reflective of pre-invasion or ~~baseline~~ near-natural states, ~~s and~~ providing~~es~~ an updated basis for developing robust diatom–environment models that are less influenced by disturbance.~~.~~ The use of field parameters collected across multiple sampling events increases confidence that the developed models reflect representative environmental conditions (Goldenberg Vilar et al. 2018; Kennedy and Buckley 2021). Such repeated-sampling approaches are rarely achieved in diatom transfer function development, particularly in remote regions such as the sub-Antarctic.

Widespread recovery of vegetation communities provides evidence for catchment scale ecosystem recovery across the island (Springer 2018; Fitzgerald et al. 2021). W~~, w~~hile quantitative runoff or nutrient time series are not available to directly extend this to limnological conditions, we are able to provide site-specific evidence from one sedimentary diatom record. At Emerald Lake (LK6), downcore diatom assemblages show a clear ecological shift coincident with the ~~onset~~introduction of rabbits (1878 CE) and ~~persistence~~their establishment on Macquarie Island ~~of rabbits~~, with *F. capucina* and *P. abundans* dominating downcore intervals ~~across this time~~ (Saunders et al. 2013). In contrast, diatom assemblages

Formatted: Font: (Default) Arial, 11 pt, Font color: Auto

Formatted: Font: (Default) Arial, 11 pt

Formatted: Font: (Default) Arial, 11 pt, Font color: Auto

Formatted: Font: (Default) Arial, 11 pt, Font color: Auto

in recent (2022) surface sediments from this site exhibit higher diversity (48 species) and greater similarity in assemblage composition to pre-rabbit sediment intervals rather than assemblages from previously collected 2006 surface sediments (15 species), which were dominated by *F. capucina* (48% relative abundance). Notably, *F. capucina* was absent from the 2022 surface sample. Together, these lines of evidence suggest that the modern calibration dataset is less influenced by organic inputs and erosion associated with the rabbit invasion period. Accordingly, we interpret the 2022 dataset as representing post-eradication recovery conditions that are moving toward, but do not necessarily fully reflect, pre-disturbance baseline states. However, further studies are needed to assess how widespread this is across the island. -

EC was shown to be the major independent driver of diatom assemblages, with strong performance in all CCA models, individually accounting for almost 50% of the variance in the full CCA model and strong explanatory power as indicted by λ_1/λ_2 (Table 34). Although EC reflects a high proportion of shared variance (Fig. 98), this is consistent with its role as an integrative measure of ionic strength and catchment inputs. The shared component primarily reflects its covariation with major ions and nutrient variables (TON and PO_4^{3-}), which are typically correlated with EC in these systems. Despite this overlap, EC retained a strong and highly significant independent effect (p = 0.001), confirming its dominant ecological influence on diatom distributions.

While PO_4^{3-}, TON, and Si each explained significant but moderate portions of individual variance (Table 34), they ~~lost~~ were no longer ~~significance~~ significant once covariation was controlled for (Table 45), meaning their explanatory power is mostly shared variance with other environmental gradients, primarily EC and each other, with negligible unique variance. - This interpretation is supported by simple linear correlations between EC and nutrient variables in coastal lakes, which show weak or absent relationships (Fig. S3). These results indicate that although nutrients and EC co-occur in coastal systems, nutrient variability is not strongly or systematically coupled to EC. Together with the VIFs (<3), variance partitioning and partial CCA results (Table 4), this supports the interpretation that the weak unique nutrient signal reflects an ecological reality in which EC exerts a first-order control on diatom assemblages, rather than a statistical artefact of collinearity. ~~While~~ Similarly, while pH explained a major and independent gradient in diatom variation within plateau lakes (Fig. 87), it did not capture assemblage changes across high-EC, high-nutrient sites. This was indicated by individual CCA results, which were

Formatted: Font: (Default) Arial, 11 pt, Font color: Auto
Formatted: Font: (Default) Arial, 11 pt, Font color: Auto
Formatted: Font: (Default) Arial, 11 pt, Font color: Auto
Formatted: Font: (Default) Arial, 11 pt, Font color: Auto
Formatted: Font: (Default) Arial, 11 pt, Font color: Auto
Formatted: Font: (Default) Arial, 11 pt, Font color: Auto
Formatted: Font: (Default) Arial, 11 pt, Font color: Auto
Formatted: Not Highlight

729 less than half of the variance explained by EC (Table 34). This, paired with the widespread oligotrophic
730 nature of plateau lakes on Macquarie Island lends strength to the independent explanatory power of EC
731 across the whole dataset.
732
733 Furthermore, pH showed poor predictive performance as a transfer function, with the lowest R^2_{boot} =
734 0.2617, and highest RMSEP = 0.63 from the WAPLS-2 model (Table 5). While this is surprising due to
735 the strong pH gradient across plateau sites, most diatoms were tolerant found across the pH gradient
736 (Fig. 11) with few some species showing clear optima for narrowed and specificbroad tolerance and pH
737 ranges. EC had the strongest performance with the WA and ML models producing the highest R^2_{boot}
738 (0.74 and 0.80, respectively) and comparable RMSEP. WA_{inv} and WAPLS-1 showed identical
739 performance, with no benefit from additional WAPLS components, which progressively increased
740 predictive error and decreased R^2_{boot}, suggesting overfitting. WA was therefore chosen over WAPLS as
741 the simpler model.
742
743 The WA EC transfer function performed better than the previously published Macquarie Island diatom-
744 conductivity transfer function (Saunders et al., 2009), with higher R^2_{boot}. However, some caution is
745 warranted when predicting across the upper EC range, where greater predictive error is evident (Fig.
746 124). This can be attributed to lower species turnover, higher variability in PO_4^{3-}, TON, and Si, and fewer
747 sites at the upper end of the nutrient and EC gradients. Further refinement of the EC transfer functions
748 could be achieved with more evenly distributed sampling across the environmental gradient. The ML
749 model, with higher R^2_{boot}, appears more capable of addressing these issues and maintains more
750 consistent predictive power across the EC range. This is likely due to its explicit curve-fitting approach.
751 By estimating individual species optima and tolerances, ML can better represent asymmetric or skewed
752 response curves (Birks 2012). The ML transfer function is therefore considered to be the preferred model,
753 although both WA and ML are robust based on comparable RMSEP.

754 **4.5 Future applications for reconstructing past climate changes**

755 The conceptual link between large-scale wind regimes and long-term limnological and ecological
756 responses in Southern Hemisphere lake systems is well established in previous studies (e.g., Saunders
757 et al. 2009; 2016; 2018; Perren et al. 2020; 2025; Van Nieuwenhuyze 2020; Humphries et al. 2021;

Formatted: Font: (Default) Arial, 11 pt, Font color: Auto
Formatted: Normal
Formatted: Font: (Default) Arial, 11 pt, Font color: Auto

Meredith et al. 2022). The data presented here builds on this existing framework, and demonstrates that i

Incorporating diatom data with seasonal and multi-year hydrogeochemical data provides a unique opportunity to comprehensively understand diatom-environment responses. By quantifying temporal variability in hydrogeochemical processes, including the role of evaporation, this study strengthens confidence that EC reflects SHW-driven sea-spray inputs rather than local lake hydrogeochemical processes. This hydrological context is critical for interpreting diatom–environment relationships and ensuring the reliability of EC as a proxy for past SHW behaviour, providing a strong foundation for future palaeoclimate reconstructions. The resulting diatom–conductivity model provides a robust and ecologically grounded framework for reconstructing long-term SHW variability on Macquarie Island and establishes an important benchmark for sub-Antarctic palaeoclimate comparisons across the region. This model will be applied in future studies to reconstruct past variability in ~~Southern Hemisphere westerly winds~~the SHW and associated hydroclimatic changes on Macquarie Island. Any future time-series monitoring of lake EC paired with local wind speed records would further allow direct assessment of the relationship between wind speed and lake salinity, including the rate of hydrogeochemical response and any wind speed thresholds required to drive measurable change.

By capturing post-eradication and near-natural ecological ~~baseline and recovered~~ conditions, the EC model developed in th~~e present~~ is study offers an improved foundation for assessing long-term wind-driven variability, as it reduces ecological noise associated with past disturbance. When applied in parallel with other proxies, such as isotopic or geochemical indicators ~~–~~(e.g. mercury and mercury isotopes (Schneider et al. 2024)), these reconstructions will contribute to a more comprehensive understanding of past SHW dynamics and their role in modulating Southern Hemisphere mid-high latitude climate, thereby providing context for understanding future changes.

Furthermore, a multiproxy approach will be valuable for independently reconstructing key climatic drivers, including precipitation, temperature, and atmospheric circulation, thereby improving interpretations of past SHW variability and helping to assess how hydroclimatic processes may modify EC signals (e.g., through dilution and enrichment). On Macquarie Island, geochemical indicators of sea-spray and dust inputs (e.g., S, Br, Ti) can help distinguish marine aerosol delivery from catchment-derived material, while glycerol dialkyl glycerol tetraethers

Formatted: Font: (Default) Arial, 11 pt, Font color: Auto

(GDGT)-biomarker reconstructions can provide an independent constraint on temperature variability. Both approaches are currently being undertaken on ~~on~~Macquarie Island lake sediment cores by our research group. Mercury (Hg) concentrations and isotopes, offer an independent proxies, for atmospheric transport and Hg deposition linked to large-scale circulation, precipitation, and the influence of seabirds, all, particularly well suited to the remote setting of Macquarie Island (Schneider et al., 2022; Guédron et al., 2020), this is also the focus of ongoing work (e.g. Schneider et al., 2024; Li et al., 2025). Although isotope (δ^2H, $\delta^{18}O$) palaeo-records are not currently available for Macquarie Island, they represent an important avenue for future research to constrain precipitation–evaporation balance. Together, these complementary proxies provide a framework to separate the relative influence of atmospheric circulation, hydroclimate, and temperature on lake systems, providing more comprehensive palaeoclimate records and interpretations.~~Furthermore, a multiproxy approach will be valuable to independently reconstruct other climatic factors such as precipitation which may also modify EC signals through dilution.~~

Formatted: Font: (Default) Arial, 11 pt, Not Bold, Font color: Auto

Formatted: Font: (Default) Arial, 11 pt, Not Bold, Font color: Auto

Formatted: Font: (Default) Arial, 11 pt, Not Bold, Font color: Auto

Formatted: Font: (Default) Arial, 11 pt, Not Bold, Font color: Auto

Formatted: Font: (Default) Arial, 11 pt, Not Bold, Font color: Auto

Formatted: Default Paragraph Font, Font: (Default) Times New Roman

5 Conclusion

This study aimed to update and re-evaluate the reliability of diatom–conductivity models as a proxy for reconstructing SHW variability on Macquarie Island by analysing diatom–environment relationships in the context of seasonal and multi-year water chemistry and isotopic ~~analysis~~analyses. Our results demonstrate that although lake hydrogeochemical processes vary locally, they remain stable seasonally and between years. Lakes near the west coast and on the western edge consistently reflect strong SSA influence, and while short-term evaporative enrichment occurs during summer, it does not obscure the dominant signal of SHW-driven SSA inputs. Accordingly, EC reliably reflects SSA deposition rather than internal lake hydrogeochemical processes, providing a firm mechanistic basis for the use of EC as an indicator of SSA deposition in palaeoclimate studies on Macquarie Island.

Diatom–environment relationships were found to be strong and ecologically coherent, supporting the development of a robust diatom–conductivity transfer function. Importantly, this study highlights the need for careful site selection, with lakes that demonstrate stable hydrogeochemical behaviour, clear SSA influence, and limited local disturbance providing the most reliable archives for reconstructing past SHW variability. The resulting transfer function offers a reliable tool for reconstructing long-term SHW dynamics, supported by well-characterised modern hydrological controls. Together, these findings

821 establish Macquarie Island as a well-constrained system for SHW reconstructions and provide a strong
822 foundation for future palaeoclimate work across the sub-Antarctic region.
823
824 **Supplementary material**
825 The Diatom Catalogue and Species List can be accessed from DOI 10.5281/zenodo.18041221
826
827 **Data availability**
828 The raw data supporting the conclusion on this work is available on request.
829
830 **Author contributions**
831 Caitlin Selfe: Conceptualization; Data curation; Formal analysis; Investigation; Methodology; Validation;
832 Visualization; Writing - original draft; Writing - review & editing.
833 Karina Meredith: Supervision; Research design; Resources; Writing - review & editing
834 Liza McDonough: Resources; Writing - review & editing
835 Justine Shaw: Supervision; Writing - review & editing
836 ~~Steve~~ Stephen Roberts: Supervision; Writing - review & editing
837 Krystyna Saunders: Conceptualisation; Supervision; Resources; Funding acquisition; Writing - review
838 & editing
839 Competing interests: The contact author has declared that none of the authors has any competing
840 interests.
841
842
843 **Acknowledgments**
844 This work was supported by ARC SRIEAS Grant SR200100005 Securing Antarctica's Environmental
845 Future. CS was supported by an AINSE Ltd. Residential Student Scholarship and acknowledges help
846 undertaking fieldwork from Maggie Smith, Sam Beale, Jez Bird, and Adam Darragh. We thank the
847 Tasmanian Parks and Wildlife Service and Australian Antarctic Division (AAS 4628) for field support
848 and access to Macquarie Island. We also thank ANSTO laboratories for sample analysis, particularly
849 Chris Vardanega and Henri Wong. This work contributes to delivering the Australian Antarctic Science
850 Decadal Strategy, in particular the Climate System and Change key priority.

References

Andersen, T., J. Carstensen, E. Hernandez-Garcia and C. M. Duarte. Ecological thresholds and regime shifts: approaches to identification. Trends in Ecology & Evolution 24 (1): 49-57. 2009.

Biester, H., F. Keppler, A. Putschew, A. Martinez-Cortizas and M. Petri. Halogen retention, organohalogens, and the role of organic matter decomposition on halogen enrichment in two Chilean peat bogs. Environmental Science & Technology 38 (7): 1984-1991. 2004.

Birks, H., D. Frey and E. Deevey. Numerical tools in palaeolimnology-progress, potentialities, and problems. Journal of paleolimnology 20: 307-332. 1998.

Birks, H. J. B. Overview of numerical methods in palaeolimnology. In Tracking environmental change using Lake sediments: Data handling and numerical techniques, 19-92: Springer. 2012.

BOM. Australian Bureau of Meterology, Climate statistics for Australian locations. https://www.bom.gov.au/climate/averages/tables/cw_300004.shtml. 2025.

Buckney, R. T. and P. A. Tyler. Reconnaissance limnology of Sub-Antarctic islands. II. Additional features of the chemistry of Macquarie Island lakes and tarns. Marine and Freshwater Research 25 (1): 89-95. 1974.

Chau, J. H., C. Born, M. A. McGeoch, D. Bergstrom, J. Shaw, A. Terauds, M. Mairal, J. J. Le Roux and B. Jansen van Vuuren. The influence of landscape, climate and history on spatial genetic patterns in keystone plants (Azorella) on sub-Antarctic islands. Molecular Ecology 28 (14): 3291-3305. doi: https://doi.org/10.1111/mec.15147. 2019.

Deng, Y. N., S. J. Roberts, K. M. Saunders, B. Perren and C. Selfe. Late-Holocene palaeoecological reconstruction of Southern Hemisphere Westerlies variability on Subantarctic Macquarie Island. The Holocene: 09596836261432461. 2025.

Evans, A. J. Some aspects of the ecology of a calenoid copepod, *Psuedoboekeela brevicaudata.* Brady, 1875, on a subantarctic island. ANARE Scientific Reports, series B, 1, Zoology: 100. 1970.

Farqan, M., L. Xiang, J. Deng, H. Chen, W. Wang, S. Yu, Z. Zhu, C. Yan, C. Huang and X. Liu. Modern surface sediment diatom assemblages and conductivity modeling in northern China. Ecological Indicators 179: 114229. 2025.

Fitzgerald, N. B., J. B. Kirkpatrick and J. J. Scott. Rephotography, permanent plots and remote sensing data provide varying insights on vegetation change on subantarctic Macquarie Island, 1980–2015. Austral Ecology 46 (5): 762-775. 2021.

Fletcher, M.-S., J. Pedro, T. Hall, M. Mariani, J. A. Alexander, K. Beck, M. Blaauw, D. A. Hodgson, H. Heijnis and P. S. Gadd. Northward shift of the southern westerlies during the Antarctic Cold Reversal. Quaternary Science Reviews 271: 107189. 2021.

Fogt, R. L. and G. J. Marshall. The Southern Annular Mode: variability, trends, and climate impacts across the Southern Hemisphere. Wiley Interdisciplinary Reviews: Climate Change 11 (4): e652. 2020.

Gasse, F., P. Barker, P. A. Gell, S. C. Fritz and F. Chalie. Diatom-inferred salinity in palaeolakes: an indirect tracer of climate change. Quaternary Science Reviews 16 (6): 547-563. 1997.

Gat, J. R. Oxygen and hydrogen isotopes in the hydrologic cycle. Annual Review of Earth and Planetary Sciences 24 (1): 225-262. 1996.

Gerritse, R. G. and R. J. George. The role of soil organic matter in the geochemical cycling of chloride and bromide. Journal of Hydrology 101 (1-4): 83-95. 1988.

Gillett, N. P., T. D. Kell and P. Jones. Regional climate impacts of the Southern Annular Mode. Geophysical Research Letters 33 (23). 2006.

Goeyers, C., D. H. Vitt and B. Van de Vijver. Taxonomic and biogeographical analysis of diatom assemblages from historic bryophyte samples from Campbell Island (sub-Antarctic). Plant Ecology and Evolution 155 (1): 107-122. 2022.

Goldenberg Vilar, A., T. Donders, A. Cvetkoska and F. Wagner-Cremer. Seasonality modulates the predictive skills of diatom based salinity transfer functions. PLOS ONE 13 (11): e0199343. doi: 10.1371/journal.pone.0199343. 2018.

Goyal, R., A. Sen Gupta, M. Jucker and M. H. England. Historical and projected changes in the Southern Hemisphere surface westerlies. Geophysical Research Letters 48 (4): e2020GL090849. 2021.

Gremmen, N. J., B. Van De Vijver, Y. Frenot and M. Lebouvier. Distribution of moss-inhabiting diatoms along an altitudinal gradient at sub-Antarctic Îles Kerguelen. Antarctic Science 19 (1): 17-24. 2007.

Guevara, S. R., A. Rizzo, R. Daga, N. Williams and S. Villa. Bromine as indicator of source of lacustrine sedimentary organic matter in paleolimnological studies. Quaternary Research 92 (1): 257-271. 2019.

Humphries, R. S., M. D. Keywood, S. Gribben, I. M. McRobert, J. P. Ward, P. Selleck, S. Taylor, et al. Southern Ocean latitudinal gradients of cloud condensation nuclei. Atmos. Chem. Phys. 21 (16): 12757-12782. doi: 10.5194/acp-21-12757-2021. 2021.

Jones, J. M., S. T. Gille, H. Goosse, N. J. Abram, P. O. Canziani, D. J. Charman, K. R. Clem, et al. Assessing recent trends in high-latitude Southern Hemisphere surface climate. Nature Climate Change 6 (10): 917-926. doi: 10.1038/nclimate3103. 2016.

Juggins, S. C2 User Guide. Software for ecological and palaeoecological data analysis and visualisation. Newcastle-uponTyne, UK: University of Newcastle. 2003.

Juggins, S. Quantitative reconstructions in palaeolimnology: new paradigm or sick science? Quaternary Science Reviews 64: 20-32. doi: https://doi.org/10.1016/j.quascirev.2012.12.014. 2013.

Keenan, H. M. Modern and fossil terrestrial and freshwater habitats on subantarctic Macquarie Island. Macquarie University Thesis. doi: https://doi.org/10.25949/24796983.v1. 1995.

Kennedy, B. and Y. M. Buckley. Use of seasonal epilithic diatom assemblages to evaluate ecological status in Irish lakes. Ecological Indicators 129: 107853. doi: https://doi.org/10.1016/j.ecolind.2021.107853. 2021.

Kong, Z., A. Prata, P. May, A. Purich, Y. Huang and S. Siems. Intensifying precipitation over the Southern Ocean challenges reanalysis-based climate estimates–Insights from Macquarie Island's 45-year record. EGUsphere 2025: 1-25. 2025.

Le Quéré, C., M. R. Raupach, J. G. Canadell, G. Marland, L. Bopp, P. Ciais, T. J. Conway, et al. Trends in the sources and sinks of carbon dioxide. Nature Geoscience 2 (12): 831-836. doi: 10.1038/ngeo689. 2009.

le Roux, P. C. and M. A. McGeoch. Rapid range expansion and community reorganization in response to warming. Global Change Biology 14 (12): 2950-2962. doi: https://doi.org/10.1111/j.1365-2486.2008.01687.x. 2008.

Lee, J. E. and S. L. Chown. Range expansion and increasing impact of the introduced wasp Aphidius matricariae Haliday on sub-Antarctic Marion Island. Biological Invasions 18 (5): 1235-1246. doi: 10.1007/s10530-015-0967-3. 2016.

Liao, M., U. Herzschuh, Y. Wang, X. Liu, J. Ni and K. Li. Lake diatom response to climate change and sedimentary events on the southeastern Tibetan Plateau during the last millennium. Quaternary Science Reviews 241: 106409. 2020.

Löffler, E. Macquarie Island: A wind-molded natural landscape in the subantarctic. Polar Geography 8 (4): 267-286. 1984.

Marchant, R., B. Kefford, J. Wasley, C. King, J. Doube and D. Nugegoda. Response of stream invertebrate communities to vegetation damage from overgrazing by exotic rabbits on subantarctic Macquarie Island. Marine and freshwater research 62 (4): 404-413. 2011.

Marshall, G. J. Trends in the Southern Annular Mode from observations and reanalyses. Journal of climate 16 (24): 4134-4143. 2003.

Maslennikova, A. V. e. Development and application of an electrical conductivity transfer function, using diatoms from lakes in the Urals, Russia. Journal of Paleolimnology 63 (2): 129-146. 2020.

McBride, T. Freshwater diatoms on sub-antarctic Macquarie Island: an ecological survey of 14 lakes. 2009.

McBride, T. P. and J. M. Selkirk. Palaeolake diatoms on sub-Antractic Macquarie Island: Possible markers of climate change. Data Symposium 1998.

Menviel, L. C., P. Spence, A. E. Kiss, M. A. Chamberlain, H. Hayashida, M. H. England and D. Waugh. Enhanced Southern Ocean CO 2 outgassing as a result of stronger and poleward shifted southern hemispheric westerlies. Biogeosciences 20 (21): 4413-4431. 2023.

Meredith, K., S. Hollins, C. Hughes, D. Cendón, S. Hankin and D. Stone. Temporal variation in stable isotopes (18O and 2H) and major ion concentrations within the Darling River between Bourke and Wilcannia due to variable flows, saline groundwater influx and evaporation. Journal of Hydrology 378 (3-4): 313-324. 2009.

Meredith, K. T., K. M. Saunders, L. K. McDonough and M. McGeoch. Hydrochemical and isotopic baselines for understanding hydrological processes across Macquarie Island. Scientific Reports 12 (1): 21266. doi: 10.1038/s41598-022-25115-3. 2022.

Molén, M. O. Geochemical proxies: Paleoclimate or paleoenvironment? Geosystems and Geoenvironment 3 (1): 100238. 2024.

Mongwe, P., L. Gregor, J. Tjiputra, J. Hauck, T. Ito, C. Danek, M. Vichi, S. Thomalla and P. M. S. Monteiro. Projected poleward migration of the Southern Ocean CO2 sink region under high emissions. Communications Earth & Environment 5 (1): 232. doi: 10.1038/s43247-024-01382-y. 2024.

Nel, W., D. W. Hedding and E. M. Rudolph. The sub-Antarctic islands are increasingly warming in the 21st century. Antarctic Science 35 (2): 124-126. 2023.

Nicholson, S.-A., D. B. Whitt, I. Fer, M. D. du Plessis, A. D. Lebéhot, S. Swart, A. J. Sutton and P. M. S. Monteiro. Storms drive outgassing of CO2 in the subpolar Southern Ocean. Nature Communications 13 (1): 158. doi: 10.1038/s41467-021-27780-w. 2022.

Oksanen, J., F. G. Blanchet, R. Kindt, P. Legendre, P. R. Minchin, R. O'hara, G. L. Simpson, P. Solymos, M. H. H. Stevens and H. Wagner. Package 'vegan'. Community ecology package, version 2 (9): 1-295. 2013.

Olivier, L. and F. A. Haumann. Southern Ocean freshening stalls deep ocean CO2 release in a changing climate. Nature Climate Change 15 (11): 1219-1225. doi: 10.1038/s41558-025-02446-3. 2025.

Peng, Y., P. Rioual and Z. Jin. A record of Holocene climate changes in central Asia derived from diatom-inferred water-level variations in Lake Kalakuli (Eastern Pamirs, western China). Frontiers in Earth Science 10: 825573. 2022.

Perren, B. B., D. A. Hodgson, S. J. Roberts, L. Sime, W. Van Nieuwenhuyze, E. Verleyen and W. Vyverman. Southward migration of the Southern Hemisphere westerly winds corresponds with warming climate over centennial timescales. Communications Earth and Environment 1 (1). doi: 10.1038/s43247-020-00059-6. 2020.

Perren, B. B., J. Kaiser, H. W. Arz, O. Dellwig, D. A. Hodgson and F. Lamy. Poleward displacement of the Southern Hemisphere Westerlies in response to Early Holocene warming. Communications Earth & Environment 6 (1): 164. doi: 10.1038/s43247-025-02129-z. 2025.

Recasens, C., D. Ariztegui, N. I. Maidana, B. Zolitschka and P. S. Team. Diatoms as indicators of hydrological and climatic changes in Laguna Potrok Aike (Patagonia) since the Late Pleistocene. Palaeogeography, Palaeoclimatology, Palaeoecology 417: 309-319. 2015.

Roberts, D., A. McMinn and D. Zwartz. An initial palaeosalinity history of Jaw Lake, Bunger Hills based on a diatom–salinity transfer function applied to sediment cores. Antarctic Science 12 (2): 172-176. 2000.

Sabbe, K., W. Vyverman, L. Ector, C. E. Wetzel, J. John, D. A. Hodgson, E. Verleyen and B. Van de Vijver. On the identity of Navicula gottlandica (Bacillariophyta), with the description of two new species Navicula eileencoxiana and Navicula bergstromiana from the Australo-Pacific region. Plant Ecology and Evolution 152 (2): 313-326. Accessed 2025/02/27/. https://www.jstor.org/stable/26672975. 2019.

Saunders, K. M., J. J. Harrison, D. A. Hodgson, R. de Jong, F. Mauchle and A. McMinn. Ecosystem impacts of feral rabbits on World Heritage sub-Antarctic Macquarie Island: A palaeoecological perspective. Anthropocene 3: 1-8. doi: https://doi.org/10.1016/j.ancene.2014.01.001. 2013.

Saunders, K. M., D. A. Hodgson and A. McMinn. Quantitative relationships between benthic diatom assemblages and water chemistry in Macquarie Island lakes and their potential for reconstructing past environmental changes. Antarctic Science 21 (1): 35-49. doi: 10.1017/S0954102008001442. 2009.

Saunders, K. M., D. A. Hodgson, S. McMurtrie and M. Grosjean. A diatom-conductivity transfer function for reconstructing past changes in the Southern Hemisphere westerly winds over the Southern Ocean. Journal of Quaternary Science 30 (5): 464-477. doi: 10.1002/jqs.2788. 2015.

Saunders, K. M., S. J. Roberts, B. Perren, C. Butz, L. Sime, S. Davies, W. Van Nieuwenhuyze, M. Grosjean and D. A. Hodgson. Holocene dynamics of the Southern Hemisphere westerly winds and possible links to CO2 outgassing. Nature Geoscience 11 (9): 650-655. doi: 10.1038/s41561-018-0186-5. 2018.

Schneider, M. A., L. Schneider, H. Cadd, Z. A. Thomas, A. Martinez-Cortizas, S. E. Connor, G. L. Stannard and S. G. Haberle. Long-term mercury accumulation and climate reconstruction of an Australian alpine lake during the late Quaternary. Global and Planetary Change 240: 104539. doi: https://doi.org/10.1016/j.gloplacha.2024.104539. 2024.

Scott, J. and J. Kirkpatrick. Rabbits, landslips and vegetation change on the coastal slopes of subantarctic Macquarie Island, 1980–2007: implications for management. Polar Biology 31 (4): 409-419. 2008.

Selkirk-Bell, J. and P. Selkirk. Vegetation-banked terraces on Subantarctic Macquarie Island: a reappraisal. Arctic, antarctic, and alpine research 45 (2): 261-274. 2013.

Selkirk, P., R. Seppelt and D. Selkirk. Subantarctic Macquarie Island: environment and biology: Cambridge University Press. 1990.

Shaw, J., A. Terauds and D. Bergstrom. Rapid commencement of ecosystem recovery following aerial baiting on sub-Antarctic Macquarie Island. Ecological Management & Restoration 12 (3): 241-244. 2011.

Springer, K. Eradication of invasive species on Macquarie Island to restore the natural ecosystem. Recovering Australian threatened species: A book of hope: 13-22. 2018.

Sterken, M., E. Verleyen, V. Jones, D. Hodgson, W. Vyverman, K. Sabbe and B. Van de Vijver. An illustrated and annotated checklist of freshwater diatoms (Bacillariophyta) from Livingston, Signy and Beak Island (Maritime Antarctic Region). Plant Ecology and Evolution 148 (3): 431-455. 2015.

Sterken, M., E. Verleyen, K. Sabbe, G. Terryn, F. Charlet, S. Bertrand, X. Boës, N. Fagel, M. De Batist and W. Vyverman. Late Quaternary climatic changes in southern Chile, as recorded in a diatom sequence of Lago Puyehue (40 40′ S). Journal of Paleolimnology 39 (2): 219-235. 2008.

ter Braak, C. J. and S. Juggins. Weighted averaging partial least squares regression (WA-PLS): an improved method for reconstructing environmental variables from species assemblages. Hydrobiologia 269 (1): 485-502. 1993.

Ter Braak, C. J. and I. C. Prentice. A theory of gradient analysis. In Advances in ecological research, 271-317: Elsevier. 1988.

Terauds, A. Changes in rabbit numbers on Macquarie Island 1974–2008. Report to Tasmanian Parks and Wildlife Service. 2009.

Thomas, Z. A., H. Cadd, C. Turney, L. Becerra-Valdivia, H. A. Haines, C. Marjo, C. Fogwill, S. Carter and P. Brickle. Westerly wind shifts drove Southern Hemisphere mid-latitude peat growth since the last glacial. Nature Geoscience. doi: 10.1038/s41561-025-01842-w. 2025.

Van de Vijer, B., Y. Freynot and L. Beyens. Freshwater diatoms from Ile de la Possession (Crozet archipelago, Subantarctica). Bibliotheca Diatomologica 46: 1-412. 2002.

Van de Vijver, B. Aulacoseira principissa sp. nov., a new ‘centric’diatom species from the sub-Antarctic region. Phytotaxa 52: 33–42-33–42. 2012.

Van de Vijver, B. Revision of the Psammothidium manguinii complex (Bacillariophyta) in the sub-Antarctic Region with the description of four new taxa. Fottea 19 (1): 90-106. doi: 10.5507/fot.2019.001. 2019.

Van Nieuwenhuyze, W. 2020. Diatom species and limnological data from 64 lakes on subantarctic Marion Island (2011) [Data set]. UK Polar Data Centre, Natural Environment Research Council, UK Research & Innovation.

Verleyen, E., D. A. Hodgson, K. Sabbe, K. Vanhoutte and W. Vyverman. Coastal oceanographic conditions in the Prydz Bay region (East Antarctica) during the Holocene recorded in an isolation basin. The Holocene 14 (2): 246-257. 2004.

Verleyen, E., D. A. Hodgson, W. Vyverman, D. Roberts, A. McMinn, K. Vanhoutte and K. Sabbe. Modelling diatom responses to climate induced fluctuations in the moisture balance in continental Antarctic lakes. Journal of Paleolimnology 30: 195-215. 2003.

Volik, O., R. M. Petrone, R. I. Hall, M. L. Macrae, C. M. Wells, M. C. Elmes and J. S. Price. Long-term precipitation-driven salinity change in a saline, peat-forming wetland in the Athabasca Oil Sands Region, Canada: a diatom-based paleolimnological study. Journal of Paleolimnology 58 (4): 533-550. 2017.